U.PORTO

FEUP FACULDADE DE ENGENHARIA UNIVERSIDADE DO PORTO

PERFORMANCE ASSESSMENT OF BUILDING FACADES INCORPORATING AN INNOVATIVE DYNAMIC THERMAL INSULATION SYSTEM THROUGH AN EXPERIMENTAL CAMPAIGN

MAARTEN NIEMAN

Dissertation submitted in partial fulfilment of the requirements for the degree of

MASTER IN CIVIL ENGINEERING — BUILDING TECHNOLOGY

Supervisor: Professora Doutora Eva Sofia Botelho Machado Barreira, PhD

Co-supervisor: Professor Doutor Ricardo Manuel dos Santos Ferreira de Almeida, PhD

SEPTEMBER 2026

MASTER'S IN CIVIL ENGINEERING 2025/2026

DEPARTMENT OF CIVIL AND GEORESOURCES ENGINEERING

Tel. +351-22-508 1901

✉ m.ec@fe.up.pt

Edited by

FACULTY OF ENGINEERING OF THE UNIVERSITY OF PORTO

Rua Dr. Roberto Frias

4200-465 PORTO

Portugal

Tel. +351-22-508 1400

✉ feup@fe.up.pt

http://www.fe.up.pt

Partial reproduction of this document is authorised provided that the Author is mentioned and reference is made to the *Master's in Civil Engineering - 2025/2026 - Department of Civil and Georesources Engineering, Faculty of Engineering of the University of Porto, Porto, Portugal, 2026*.

The opinions and information included in this document represent solely the views of the respective Author, and the Editor cannot accept any legal or other responsibility for any errors or omissions that may exist.

This document was produced from an electronic version provided by the respective Author.

Dedicated to my parents, siblings, friends and teachers. Your support, encouragement and guidance have helped me throughout my life.

"You miss 100% of the shots you don't take."

– Wayne Gretzky

ACKNOWLEDGEMENTS

To begin, I would like to express my deepest gratitude to who has helped me through this academic period and giving me the opportunity to contribute to this research.

In particular, I would like to show my heartfelt and appreciation to my supervisors, Professora Doutora Eva Sofia Botelho Machado Barreira and Professor Doutor Ricardo Manuel dos Santos Ferreira de Almeida. I could not have wished for any more patient, understanding and kind professors that helped me through this academic journey, even when times were tough for me. Without your guidance this academic period would have been much harder, so therefore my utmost gratitude to the both of you.

A thank you to everyone else who made this journey possible:

To Engineer Eduardo Costa, for all the help and support in the lab and the many enriching conversations we shared throughout this past semester. His encouragement and kindness made this chapter much more meaningful.

To Manuel João Pereira Ribas, it was a pleasure collaborating with you and running my experiments alongside yours. I am happy to have had the pleasure to your support and your friendship during this time.

A special thanks to the entity that made this research possible. This work is financed by FEDER funds through COMPETE2030 and with financial support of FCT, I.P., within the framework of the project i-DINSystem- Intelligent and Dynamic thermal INsulation System for adaptive modular façades, with nr. 15129, operation code at the Funds Platform COMPETE2030-FEDER-00879100 e ref.ª FCT- 2023.182257.ICDT.

To my parents, supporting me though all these years. Their kind words and listening ear helped me more than they might realize. Without them my journey in Portugal wouldn't have been possible. Therefore, my eternal gratitude and love to them.

Finally, to all my friends and family, thank you for supporting and believing in me throughout all these years. You are an irreplaceable part of my life, and for that, I am truly grateful.

Forever grateful.

ABSTRACT

Dynamic thermal insulation systems (DTIS) offers a promising approach to reducing heat stress in building envelopes through mechanically ventilated air cavities within double leaf walls. However, the effectiveness of such systems depends heavily on achieving an optimal ventilation configuration, an aspect that remains insufficiently characterised in existing research. This study investigated the influence of fan quantity, fan positioning, and opening size on the air changes per hour within a DTIS wall cavity, and examined the contribution of the stack effect to overall ventilation performance.

The research was conducted with a double brick leaf wall specimen fitted with a climatic chamber. Using carbon dioxide as a tracer gas in accordance with the concentration decay method defined in ISO 12569:2017. Twelve data loggers were first calibrated to identify those offering the highest measurement accuracy, which were then distributed within the wall cavity, at the inlet and outlet and in the ambient environment. A dedicated fan and wiring system was created to allow flexible repositioning between configurations. Ten experiments were conducted across six configurations, systematically varying fan number, spatial arrangement, and opening size. Each following a repeated injection, settlement, and decay procedure. The results showed that fan positioning exerted a great influence on internal ACH, with adjacent fan arrangements outperforming distributed arrangements using an equal number of fans by up to 59.6%. Increasing fan quantity and enlarging opening size also improved ACH, although to a lesser extent. The stack effect, isolated through comparison of chamber active and chamber inactive conditions, contributed a modest but measurable 18.7% increase in internal ACH. High repeatability was confirmed through direct repetition of selected configurations.

Overall, the relative influence of fan quantity, positioning, opening size, and the stack effect on DTIS ventilation performance was successfully characterised, and an optimal fan configuration was identified within the tested wall assembly. These findings indicate that fan positioning is the primary design consideration for optimising DTIS ventilation performance, offering practical guidance for the design of ventilated building envelopes.

KEYWORDS: Dynamic thermal insulation system (DTIS), ventilated air cavity, fan configuration, stack effect, air changes per hour (ACH), tracer gas method

RESUMO

A investigação foi realizada num provete de parede de dupla folha de tijolo, equipado com uma câmara climática, utilizando dióxido de carbono como gás traçador, de acordo com o método de decaimento de concentração definido na norma ISO 12569:2017. Doze sensores de CO2 foram inicialmente calibrados para identificar os mais precisos, sendo depois distribuídos na cavidade da parede, na entrada e saída de ar, e no ambiente exterior. Foi ainda concebido um sistema de ventiladores e cablagem que permitia o reposicionamento flexível entre configurações. Realizaram-se dez experiências em seis configurações distintas, variando sistematicamente o número de ventiladores, a sua disposição espacial e a dimensão das aberturas, seguindo cada uma um procedimento repetido de injeção, estabilização e decaimento.

Os resultados demonstraram que a posição dos ventiladores exerceu a maior influência sobre o ACH interno, com configurações de ventiladores adjacentes a superarem configurações distribuídas com o mesmo número de ventiladores em até 59,6%. O aumento do número de ventiladores e da dimensão das aberturas também melhorou o ACH, ainda que em menor grau. O efeito de chaminé, isolado através da comparação entre as condições com câmara climática ativa e inativa, contribuiu com um aumento modesto, mas mensurável, de 18,7% no ACH interno. A elevada repetibilidade dos resultados foi confirmada através da repetição direta de configurações selecionadas.

Em suma, foi possível caracterizar a influência relativa do número de ventiladores, da sua posição, da dimensão das aberturas e do efeito de chaminé no desempenho de ventilação do DTIS, tendo sido identificada uma configuração ótima dentro do âmbito do provete testado. Estes resultados indicam que a posição dos ventiladores constitui a principal variável de projeto para otimizar o desempenho de ventilação de sistemas DTIS, fornecendo orientações práticas para o desenho de envolventes de edifícios ventiladas.

PALAVRAS-CHAVE: Sistema de isolamento térmico dinâmico (DTIS), cavidade de ar ventilada; configuração de ventiladores, efeito de chaminé; renovações de ar por hora (ACH), método do gás traçador

TABLE OF CONTENTS

ACKNOWLEDGEMENTS I

ABSTRACT III

RESUMO V

1 INTRODUCTION 1

1.1 PROBLEM CONTEXT 1

1.1.1 Research Gap 2

2 PERFORMANCE OF DYNAMIC THERMAL INSULATION SYSTEMS 5

2.1 THE OVERHEATING CHALLENGE IN BUILDINGS 5

2.1.1 Health and Social Consequences 6

2.1.2 Climate Change as an Accelerating Driver 6

2.1.3 The building sector and climate change 7

2.1.4 Growing demand for residential cooling 8

2.2 ADAPTIVE FACADES AND DYNAMIC THERMAL INSULATION SYSTEMS 10

2.2.1 Concepts of adaptive facades 10

2.2.2 Dynamic Thermal Insulation Systems 11

2.2.3 Performance and benefits 12

2.3 AIRFLOW MEASUREMENT IN WALL CAVITIES 13

2.3.1 Importance of Airflow Characterisation 13

2.3.2 Tracer Gas Methodology 14

2.3.3 Carbon Dioxide as a Tracer Gas 16

2.3.4 Implications for dynamic insulation system optimization 17

3 METHODOGY 19

3.1 WALL AND CLIMATIC CHAMBER 19

3.2 TRACER GAS MONITORING 21

3.2.1 Data Logger Configuration and Calibration 22
3.2.2 Tracer gas injection 25
3.3 EXPERIMENTAL SETUP 26
3.3.1 Placement of the loggers 26
3.3.2 Fans wiring 28
3.3.3 Configurations 30
3.4 TEST PROCEDURES 31
3.4.1 Injection 32
3.4.2 Settlement 33
3.4.3 Decay 33
3.4.4 Monitoring Procedures 34
4 RESULTS 35
4.1 EXPERIMENTS OVERVIEW 35
4.1.1 Experiment 1 36
4.1.2 Experiment 2 39
4.1.3 Experiment 3 39
4.1.4 Experiment 4 40
4.1.5 Experiment 5 42
4.1.6 Experiment 6 43
4.1.7 Experiment 7 44
4.1.8 Experiment 8 46
4.1.9 Experiment 9 47
4.1.10 Experiment 10 47
4.2 DISCUSSION OF THE DATA 49
4.2.1 Comparison of the test 50
4.2.2 Comparison of the configurations 52
5 CONCLUSION 56
5.1 SUMMARY OF THE METHODOLOGY 56
5.2 RESULTS AND KEY FINDINGS 57

5.3 IMPLICATIONS AND DISCUSSION 57

5.4 RECOMMENDATIONS FOR FUTURE RESEARCH 58

LIST OF FIGURES

Figure 1: CO_2 emissions in buildings 2010-2023 (left) and share of buildings in global energy and process emissions in 2023 (right) [6] 7
Figure 2: Schematic representation of the dynamic wall system studied by Almeida et al. [10]. 11
Figure 3. Thermal resistance of the DTIS wall over time for the different states 12
Figure 4. Typical tracer gas decay rate measurement. (a) Measured tracer decay and (b) logarithmic plot of (a). 15
Figure 5: Cross-section of the DTIS wall 20
Figure 6: Image of the DTIS wall with the openings sealed 21
Figure 7: Enclosure for logger configuration 22
Figure 8: Plot of the natural CO2 decay for each logger 23
Figure 9: Suitability ranges of the loggers in ACH (h-1) 24
Figure 10: CO_2 gas cannister and DTIS wall setup 25
Figure 11: Placement of the loggers 27
Figure 12: Wiring diagram 29
Figure 13: Configurations 31
Figure 14: Phases of the decay experiment 32
Figure 15: Comparison of regression graphs under different preconditions 36
Figure 16: Configuration 1 38
Figure 17: Configuration 2 41
Figure 18: Configuration 3 42
Figure 19: Configuration 4 43
Figure 20: Configuration 5 45
Figure 21: Configuration 6 48
Figure 22: Overview of the tests in ACH (h^{-1}) 49
Figure 23: Comparison chamber status 51
Figure 24: Comparison of the configurations in average ACH (h^{-1}) 52
Figure 25: Comparison of positioning of the fans in ACH (h^{-1}) 53

LIST OF TABLES

Table 1: Ranking of the loggers 24
Table 2: Results of experiment 1 in ACH (h-1) 39
Table 3: Results of experiment 3 in ACH (h-1) 40
Table 4: Results of experiment 4 in ACH (h-1) 41
Table 5: Results of experiment 5 in ACH (h-1) 43
Table 6: Results of experiment 6 in ACH (h-1) 44
Table 7: Results of experiment 7 in ACH (h-1) 45
Table 8: Results of experiment 8 in ACH (h-1) 46
Table 9: Results of experiment 9 in ACH (h-1) 47
Table 10: Results of experiment 10 in ACH (h-1) 48

SYMBOLS, ACRONYMS AND ABBREVIATIONS

ACH	[h^{-1}]	Air changes per hour
t	[h][s]	Time
Q	[m^3/s]	Flow rate
V	[m^3]	Volume
R	[$m^2 \cdot K/W$]	Thermal resistance value
λ	[$W/m \cdot K$]	Thermal conductivity
U	[$W/(m^2.K)$]	Thermal transmittance
T	[ºC]	Temperature
f	[Hz]	Frequency

UHI	Urban Heat Island
CO_2	Carbon Dioxide
AF	Adaptive Facades
$UNEP$	United Nations Environment Programme
$DTIS$	Dynamic Thermal Insulation System
AC	Alternating Current
DC	Direct current
PPM	Parts per million
$ACH\ INT$	Internal hourly exchange rate

Ref	References
Tab	Table

1 INTRODUCTION

1.1 PROBLEM CONTEXT

The global building and construction sector stands at the centre of two intersecting crises: the accelerating effects of climate change and the rapid growing demand for indoor thermal comfort. In 2023, buildings were responsible for approximately 34% of global energy related CO_2 emissions and 32% of total final energy consumption. Operational emissions from buildings reached a record high of 9.8 gigatons of CO_2 equivalent in that year alone. A trajectory fundamentally incompatible with the net zero targets established under the Paris Agreement. Simultaneously, global average temperatures have already exceeded 1.5 °C above pre-industrial levels, intensifying the frequency and severity of heatwaves and extending the periods during which buildings are exposed to thermal stress.

The consequences of these changes for the built environment are particularly acute. Overheating, defined as the condition in which indoor operative temperatures persistently exceed the upper limits of occupant thermal comfort, is now recognised as a significant and growing problem across European building stock, even in temperate climates that were historically associated with heating-dominated performance requirements. The conventional response to overheating is mechanical cooling. However, air conditioning systems already account for nearly 20% of global electricity consumption in buildings, and their use is projected to more than triple by 2050 if current trends continue. This creates a negative feedback loop in which greater heat stress drives higher energy consumption for cooling, which in turn increases greenhouse gas emissions and further accelerates climate change.

Passive design strategies that reduce or eliminate the need for mechanical cooling are therefore of utmost importance. Among these, the thermal performance of the building envelope plays a central role. While high levels of static thermal insulation are effective in reducing winter heating loads, they can exacerbate overheating in summer by preventing the release of heat accumulated within the building fabric during the day. This fundamental limitation of static insulation has motivated research into dynamic thermal insulation systems (DTISs), which can modulate the thermal resistance of the wall assembly in response to varying environmental conditions, maintaining high insulation during cold periods while switching to a more conductive configuration to promote passive heat dissipation during overheating events.

1.1.1 Research Gap

Although the concept of dynamic thermal insulation has attracted growing research interest, the published literature remains limited in several important respects. The majority of existing studies are simulation-based, with experimental validation representing a smaller share of the available evidence. Laboratory investigations have confirmed that ventilating the air cavity of a multi-layer wall assembly can reduce its thermal resistance by up to 60%, demonstrating the technical viability of the DTIS principle. However, the performance of such systems in geometrically realistic wall configurations, particularly those based on traditional masonry construction rather than purpose-built laboratory panels, has received comparatively little attention.

A further gap concerns the characterisation of airflow within the wall cavity itself. The thermal effectiveness of a ventilated cavity DTIS is directly dependent on the magnitude and spatial distribution of airflow through the cavity: insufficient airflow fails to displace the thermally still boundary layer, while non-uniform flow creates zones of limited convective exchange that reduce the overall performance of the system. The relationship between fan operating parameters, cavity geometry, and effective air change rate has not been systematically characterised for double leaf brick wall configurations. Without this empirical foundation, the optimisation of DTIS operation for the large proportion of European building stock constructed from brick masonry cannot be adequately addressed.

The tracer gas methodology standardised in ISO 12569:2017 provides an established and precise framework for measuring airflow rates in enclosed spaces. The use of carbon dioxide (CO_2) as a tracer gas, monitored by compact data-logging sensors deployed within the cavity, offers a practical and minimally intrusive means of characterising cavity airflow across a range of ventilation conditions. This approach has been validated for building-zone measurements but has not been systematically applied to the cavity of a double-leaf brick wall in a DTIS context.

2
PERFORMANCE OF DYNAMIC THERMAL INSULATION SYSTEMS

2.1 THE OVERHEATING CHALLENGE IN BUILDINGS

Overheating in buildings refers to conditions which indoor temperature exceed the limit associated with occupant thermal comfort, typically defined as operative temperatures above a value of 24 °C to 30 °C under local adaptive comfort models. This phenomenon has intensified in recent decades because of converging pressures: rising baseline temperatures driven by climate change, rapid urbanisation, and the increase of internal heat gains from occupants and equipment. While overheating was historically regarded as a problem confined to warm climates, it is now recognised as a concern across several regions of Europe, including countries that were traditionally more focused on cold-season performance [1].

The built environment plays a big role in amplifying heat stress. Buildings retain heat absorbed during the day and release it slowly overnight, thus reducing the effectiveness of the natural nocturnal cooling of interior spaces. This effect is amplified in dense urban environments, where the urban heat island (UHI) phenomenon increases ambient temperatures relative to surrounding rural areas [2] The UHI arises from the replacement of natural vegetation with heat absorbing surfaces such as concrete, brick and asphalt, the design of urban canyons that trap longwave heat radiation and heat emissions from vehicles, industry and air conditioning. Urban centres across Europe regularly record nighttime temperatures several degrees above those of surrounding rural areas; London and Paris, can be approximately 4 °C warmer at night [2].

2.1.1 Health and Social Consequences

Extended periods of exposure to increased indoor temperatures may cause serious thermal discomfort and creates a threat to physical and mental wellbeing. Population groups such as: the elderly, young children and individuals with pre-existing cardio vascular or respiratory conditions have a elevated mortality risk to these factors. A study assessing mortality risks associated with UHI's of 93 European cities found that during extreme heat periods, urban heat islands were associated with a 45% median increase in mortality risk compared to regular conditions [3].

The health consequences go beyond direct thermal stress and discomfort. Cases such as decreased labour productivity and increased rates of workplace accidents come paired with extended periods of intense heat. Research suggests that 46% of hospitals and 43% of schools are located in areas with strong UHI effects exceeding 2°C, placing their most vulnerable users at higher risk [4]. These outcomes are projected to worsen with future climate change trends, with heatwaves to be expected to increase in frequency, duration and severity, especially in southern Europe.

2.1.2 Climate Change as an Accelerating Driver

The intergovernmental Panel on Climate Change (IPCC) has confirmed with high certainty that human caused greenhouse gas emissions have increased global mean surface temperatures by roughly 1.1 °C above pre-industrial revolution levels [1], with further predicted warming. In 2024, global average temperatures reached 1.5 °C above ordinary temperatures for the first time on a full year basis. The years between 2015 and 2025 we confirmed by the World meteorological Organisation to be the warmest decade that has been globally recorded, with record breaking temperatures have been increasing steadily across Europe, North Africa, the middle east and Asia.

These changes have important implications for the building performance. Rising outdoor temperatures increases heat through building facades and reduce the effectiveness of natural ventilation during hot periods as the temperature difference between indoor and outdoor environments becomes smaller. As a result, inhabitants are increasingly exposed to a greater risk of thermal discomfort and overheating. This issue is especially significant for existing buildings. Many of which were designed according to climatic conditions that no longer match current or future realities. Without any adaptation measures, including altering building design and the retrofit of existing real estate, overheating is expected to become an increasingly serious challenge in the coming decades [5].

2.1.3 The building sector and climate change

The building and construction sector is one of the most major contributors to global energy demand and greenhouse gas emissions. According to the Global Status Report for Buildings and Construction published jointly by the United Nations Environment Programme (UNEP), in 2023 buildings were responsible for approximately 32% of total global energy demand and 34% of global energy related CO_2 emissions. [6]. Operating emissions from buildings reached a record level of 9.8 gigatons of carbon dioxide in 2023, while embodied carbon associated with the manufacture of construction materials accounted for an added 2.9 gigatons (Figure 1).

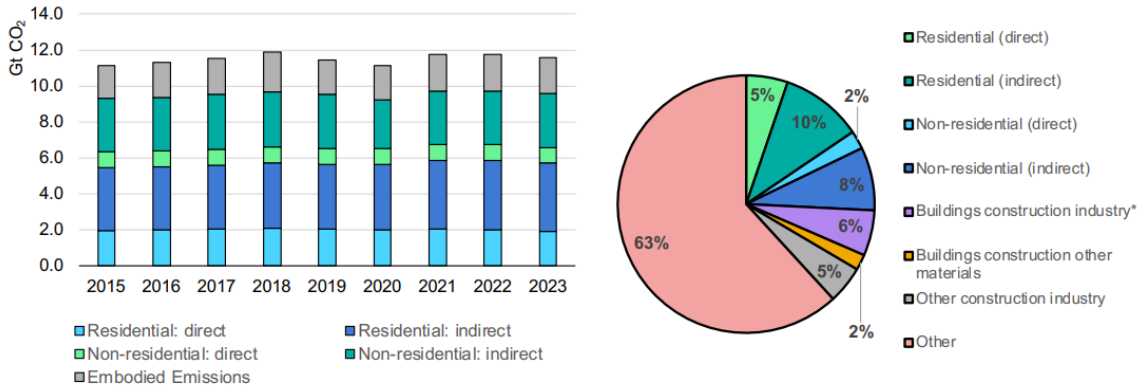


Figure 1: CO_2 emissions in buildings 2010-2023 (left) and share of buildings in global energy and process emissions in 2023 (right) [6]

Despite growing awareness and policy improvements, the trajectory of building sector emissions remains incompatible and unaligned with the objectives of the Paris Agreement. Between 2015 and 2023 the CO_2 emissions from building operations increased by a value of 5.4%. The sector now accounts for roughly 37% of global operational energy and process related CO_2 emissions when construction activities are included. This represents a massive structural challenge for climate policy.

A key driver of this trend is the continued expansion of global building stock. In 2023 over five billion square meters of new floor area were added worldwide, mainly in emerging economies [6]. An additional 2.4 billion square meters of floor space were added in countries without any building energy codes, meaning a large proportion of new construction is not subject to minimum building performance requirements. Energy intensity in buildings, measured as annual energy consumption per unit of floor area, decreased by only 9.5% since 2015, well below the 18.2% reduction required to meet 2030 targets [6].

2.1.4 Growing demand for residential cooling

Within the building sector, cooling is currently the fastest-growing end use in terms of energy demand. According to the International Energy Agency, energy demand for space cooling has risen at an average rate of approximately 4% per year since 2000, and this growth shows no sign of abating. Air conditioning and electric fans already account for nearly 20% of total global electricity consumed in buildings. The global stock of air conditioners has more than tripled since 2000, reaching over 1.5 billion residential units in 2022.

The IEA projects that, without major policy intervention, global demand for space cooling will more than triple by 2050, requiring new electricity generation capacity equivalent to the combined installed capacity of the United States, the European Union and Japan today. In its World Energy Outlook 2024, the IEA modelled that air conditioning will generate over 1,200 TWh of additional global demand for electricity by 2035 under current policy trajectories [8]. By 2050, approximately two-thirds of the world's households could own an air conditioning unit, with China, India, and Indonesia together accounting for half of all units.

This growth carries major environmental and systemic consequences. The operation of air conditioning systems demands large amounts of electricity. The method for generation remains mainly dependant on fossil fuel in many regions. During the heat waves of summer 2024, cooling demand doubled electricity demand growth in China during August and September relative to the same period in 2023 [8]. The cooling driven peaks also threaten grid stability and affordability, especially in developing countries where infrastructure is less advanced. Furthermore, the cooling gasses known as Freon and Puron, used in conventional air conditioning systems have global warming potentials orders of magnitude higher than CO_2, adding environmental concern [9]. These topics reinforce the urgency of developing passive and low energy alternatives to mechanical cooling.

Addressing the challenge of overheating and rising energy demand for cooling requires a multitude of interventions operating across multiple scales. At the urban level, strategies such as urban greening, cool pavements and appropriate building massing can reduce temperatures and minimize the UHI effect. At smaller scale, building level, measures include improving the thermal performance of the envelope. Deploying effective cooling systems, enhancing thermal mass to temperature fluctuations and enabling controlled natural ventilation during cooler periods [10].

Passive and low energy cooling strategies are particularly attractive because they reduce the need for energy intensive systems, lower operating costs and improve resilience during periods of power outages. A study of facade retrofitting measures found that architectural interventions targeting the building envelope can reduce energy consumption for heating and cooling by up to 50% [9]. The choice for the most efficient strategy is highly dependent on the context and must account for local climatic conditions, building typology, occupancy patterns and the interaction between heating and cooling demands across seasons.

An insight from recent research is that traditional insulation presents a trade off: while high thermal resistance reduces heat loss during winter, it can increase overheating chances during summer by entrapping heat within the building [11]. This limitation has motivated the development of adaptive and dynamic measures to thermal insulation, which can shift the thermal behaviour of the envelope in response to changing conditions rather than optimising for a single reason.

2.2 ADAPTIVE FACADES AND DYNAMIC THERMAL INSULATION SYSTEMS

2.2.1 Concepts of adaptive facades

A major challenge in building envelope design is the need to satisfy multiple, sometimes contradictory, functional requirements across a wide range of conditions. A facade must simultaneously manage heat transfer, solar radiation, moisture, air movement and daylight, while satisfying structural, aesthetic, and durability criteria [11]. Traditional facades are designed to a fixed set of properties optimised for average or dominant conditions, which means they inevitably underperform in conditions that deviate from this optimum.

Adaptive facades (AFs) have emerged as a response to this limitation. Broadly defined, an adaptive facade is a multi-parameter, high-performance building envelope system capable of changing its properties, behaviour, or configuration in real time, in response to external climatic stimuli or internal occupancy conditions [12]. This adaptation can be achieved through mechanical means, chemical phase transitions, electrochromic or thermochromic materials, or controlled ventilation of internal cavities [13]. The defining characteristic is dynamic responsiveness: the facade does not behave as a passive, static barrier but acts as a controlled interface between the interior and the exterior.

Despite their considerable potential, adaptive facades face significant barriers to wider adoption. Attia identified two primary obstacles: the lack of standardised performance evaluation methos suited for the dynamic nature of these systems, and the multiple regulatory and technical difficulties that must be overcome before market suitability [11]. Conventional static performance metrics such as U-value and solar heat gain coefficient are inadequate for characterising the performance of systems whose thermal properties change over time. This necessitates new experimental protocols, long term monitoring datasets, and adapted numerical simulation tools.

2.2.2 Dynamic Thermal Insulation Systems

Dynamic Thermal Insulation Systems (DTIS) represent a specific category of adaptive facades in which the thermal resistance of the wall assembly can be modulated in a controlled manner. The underlying concept was identified as early as the mid-nineteenth century by Pettenkoffer at the University of Munich, who investigated the thermal properties of porous walls through which air could circulate [14]. Several wall designs incorporating controlled air circulation were subsequently introduced in the early twentieth century, though widespread research interest in the topic is more recent.

In the context of modern-day building physics, a DTIS operates by switching between two distinct states depending on occurring conditions [9,14]. In the insulation state, the air cavity or permeable layer within the wall construction is closed or static, and the assembly behaves as a conventional insulating wall, minimising heat transfer between the interior and the exterior. In the conductive state, airflow through the cavity or porous material is activated, enhancing convective heat exchange and effectively reducing the thermal resistance of the assembly. This reduction in thermal resistance is desirable in summer overheating scenarios, where it allows excess heat stored within the wall to be expelled to the cooler external environment during night-time hours, or to enhance heat transfer towards the exterior whenever the exterior is cooler than the interior. Figure 2 shows an example of a DTIS.

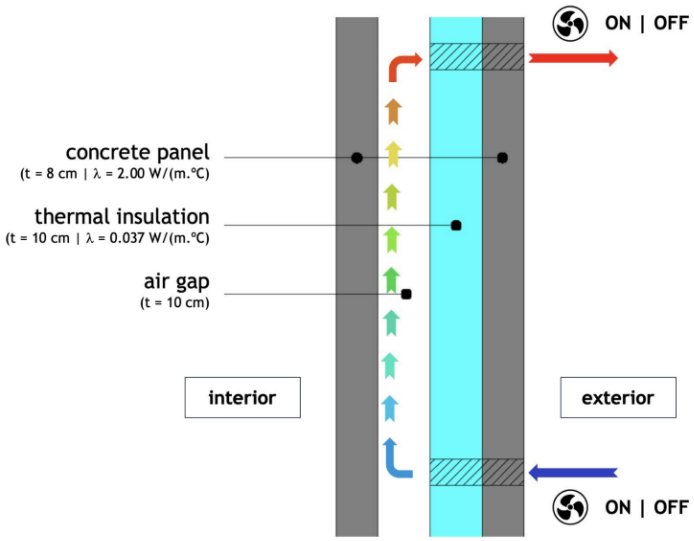


Figure 2: Schematic representation of the dynamic wall system studied by Almeida et al. [10].

The ventilation of the air cavity can be driven by natural buoyancy forces also known as the stack effect. Added; mechanical fans, or a hybrid system combining both approaches, can provide higher airflow within the wall. The direction of airflow and its relationship to the heat flux through the wall can be classified into two principal configurations [9]. In the pro-flux configuration, the airflow and the net heat flux travel in the same direction, which tends to reduce thermal resistance. In the contra-flux configuration, the airflow moves in the direction opposite to the heat flux, which can create a counter-exchange effect that further reduces effective heat loss to the interior while venting heat to the exterior.

2.2.3 Performance and benefits

The experimental characterisation of DTIS performance was demonstrated comprehensively by Almeida and Barreira et al. [10], who developed a prototype wall assembly based on a ventilated internal air gap and tested it in a Hot Box laboratory apparatus. Their prototype consisted, from interior to exterior, of an 8 cm concrete panel, a 10 cm air gap, a 10 cm thermal insulation panel, and a further 8 cm concrete panel. Mechanical ventilation of the air gap at a maximum airflow of 52 m^3/h was activated to switch the system between insulation and conductive states. Laboratory tests conducted in accordance with ISO 9869-1:2014 over seven-day periods for each state yielded thermal resistance values of 3.89 m^2 °C/W in the insulation state and 1.56 m^2 °C/W in the conductive state, corresponding to a reduction in thermal resistance of approximately 60% [10]. Figure 3 illustrates the evolution of thermal resistance over the measurement period for both states.

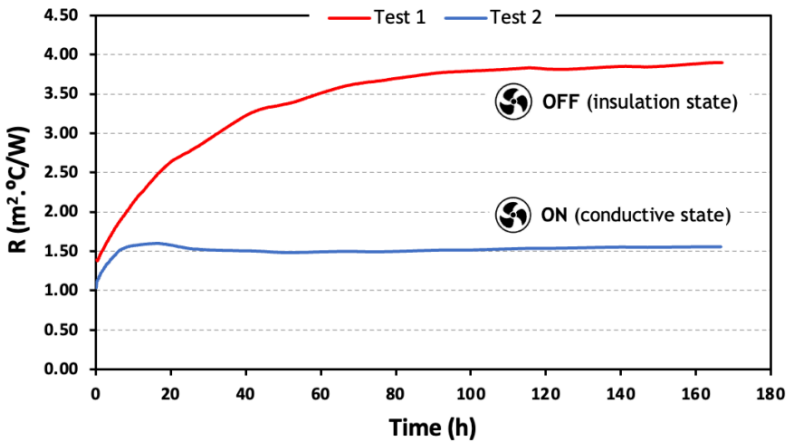


Figure 3. Thermal resistance of the DTIS wall over time for the different states

The study also confirmed that DTISs implemented in high mass buildings produce a greater impact than in lower mass buildings. Added that the north oriented facade, receiving no direct solar radiation, benefits most consistently from the DTIS due to the persistent negative temperature differential between the interior and exterior surfaces during summer nights. These findings underscore the significant potential of DTIS technology to contribute to the mitigation of overheating in buildings while avoiding the energy penalty associated with mechanical cooling.

2.3 AIRFLOW MEASUREMENT IN WALL CAVITIES

2.3.1 Importance of Airflow Characterisation

The thermal performance of a dynamic thermal insulation system is critically dependent on the rate and uniformity of airflow through the cavity or permeable layer. The relationship between airflow velocity and effective thermal resistance is non-linear: insufficient airflow fails to displace the thermally stagnant boundary layer within the cavity, while excessive airflow may introduce excessive heat from warmer exterior air or create pressure-driven infiltration pathways that undermine the building's airtightness [9]. Accurate characterisation of the airflow regime within the wall is therefore a prerequisite for both the calibration of numerical simulation models and the operational optimisation of the dynamic insulation system under real conditions.

Airflow within a cavity wall can be complex, involving laminar and turbulent flow regimes, spatial non-uniformities arising from the geometry of the cavity and the distribution of inlet and outlet apertures, and time-varying behaviour driven by fluctuations in fan speed, wind pressure, and temperature-induced buoyancy forces. Experimental measurement of these airflows is therefore non-trivial and requires methods capable of capturing both the magnitude and the spatial distribution of flow rates within the enclosed cavity environment.

2.3.2 Tracer Gas Methodology

Tracer gas methods are one of the most established and reliable techniques for measuring airflow rates in closed spaces. A quantity of an inert, non-toxic and easily detectable gas is introduced into a confined space of interest. Its subsequent concentration is monitored over time. The evolution or decay of the concentration, combined with knowledge of the space volume and the gas injection rate, allows the volumetric airflow rate through the space to be calculated [15].

The ISO 12569:2017 standard, provides the definitive international framework for the application of tracer gas methods to the determination of specific airflow rates in buildings. The standard establishes three distinct measurement methods, each suited to different experimental conditions [15].

The concentration decay method involves injecting the tracer gas until a uniform initial concentration is established throughout the zone, then ceasing the injection and monitoring the subsequent decay of concentration as the tracer is diluted by the incoming airstream. This method is particularly suitable for steady or quasi stable ventilation conditions and produces a straightforward exponential decay curve from which the air change rate can be extracted by linear regression on the logarithm of concentration versus time [15,17]. Figure 4 portrays a plotted graph of the mentioned decay

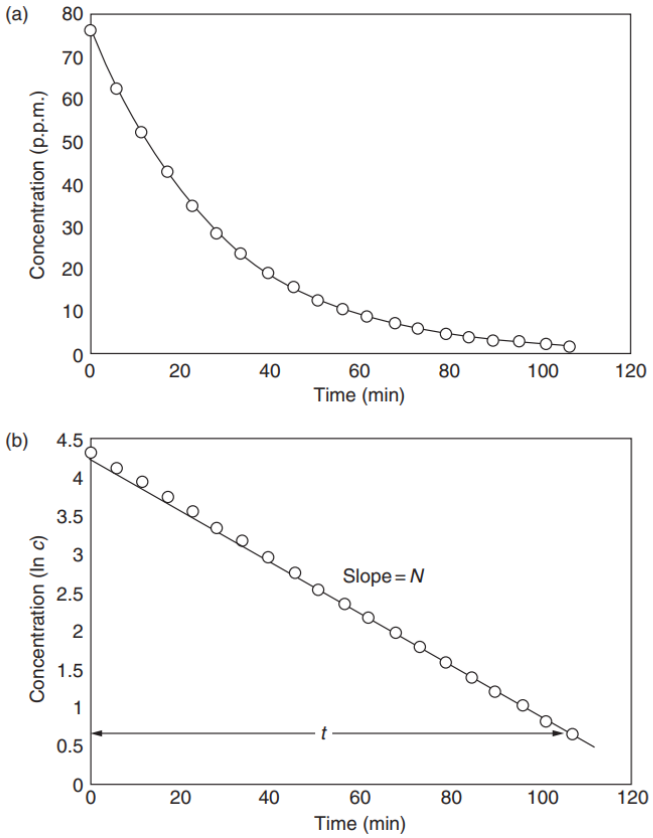


Figure 4. Typical tracer gas decay rate measurement. (a) Measured tracer decay and (b) logarithmic plot of (a).

The air change rate and corresponding volumetric airflow through the cavity are determined by applying Equation 1, which is derived from the logarithmic transformation of the exponential concentration decay curve. This linearisation allows the decay rate constant to be extracted through linear regression, from which the air change rate per hour (ACH) and the associated airflow rate are subsequently calculated:

$$ln\, c - lc\, ln\, c_0 = -\left(\frac{Q}{V}\right) t \quad (1.1)$$

Where c_0 = the concentration of tracer gas at time $t = 0$ and $Q/V = N$ = air change rate (ACH)

Equation 1: Logarithmic decay formula

The injection method involves injecting the tracer gas at a constant, known rate and monitoring the concentration achieved once equilibrium between injection and removal is completed. The airflow rate is calculated from the ratio of the injection rate to the equilibrium concentration [15]. This method is well suited to conditions where airflow rates are stable over time and have minimal fluctuations.

The constant concentration method involves continuously adjusting the tracer gas injection rate to maintain a fixed target concentration within the zone, monitoring the required injection rate to maintain this equilibrium. This technique is particularly useful for highly variable ventilation conditions, as it provides a time resolved record of airflow rate throughout the measurement period [15]. It is, however, more demanding in terms of instrumentation and control methods.

2.3.3 Carbon Dioxide as a Tracer Gas

Carbon dioxide (CO_2) is one of the most widely used tracer gases for ventilation measurement in the built environment, owing to its non-toxicity, low cost, natural presence in the atmosphere, and the wide availability of accurate, affordable infrared sensor technology [17]. In the context of measuring airflow within a wall cavity, CO_2 offers important practical advantages: it can be injected in small quantities, it does not react with the wall materials and its concentration can be monitored with high temporal resolution using compact data-logging sensors that can be installed within the cavity without significantly disturbing the flow field.

Cui et al. [17] validated the CO_2 concentration decay method for air change rate measurement in building spaces and demonstrated good agreement between measurements obtained using CO_2 and those obtained using conventional tracer gases such as sulphur hexafluoride (SF_6). The main consideration when using CO_2 as a tracer gas is the need to account for the background concentration present in ambient air (approximately 400 to 420 ppm under ordinary atmospheric conditions). Thus, must be subtracted from measured concentrations before applying the decay analysis.

For the current research, CO_2 loggers will be deployed within the air cavity of a double leaf brick wall to monitor the evolution of CO_2 concentration during decay experiments. The decay method defined in ISO 12569:2017 and [15] will be applied to determine the volumetric airflow rate through the cavity under different fan operating conditions. This method allows the relationship between fan speed and effective air change rate to be established, providing the experimental data necessary to calibrate numerical airflow models and to define the operational parameters of the dynamic insulation system.

2.3.4 Implications for dynamic insulation system optimization

The data obtained through tracer gas measurements serve multiple roles in the development and validation of a dynamic thermal insulation system. First, they provide direct evidence of the air change rates achievable within the cavity under different operating conditions, which can be used to select appropriate fan specifications and control strategies. Second, they allow the uniformity of airflow distribution within the cavity to be assessed: non-uniform flow, with dead zones or preferential flow paths, reduces the effectiveness of the dynamic insulation by limiting convective heat exchange over parts of the wall area. Third, the measured airflow data can be used as input to couple airflow-heat transfer simulations to predict the thermal performance of the wall system under real operating conditions [9].

Previous research on ventilated cavity walls and breathing walls has demonstrated that the thermal coupling between the interior and exterior environments is strongly dependent on the airflow velocity within the cavity. Experiments have shown that increasing the airflow velocity from 0 to 12 mm/s in a breathing wall configuration progressively enhances thermal coupling and reduces the effective thermal resistance of the wall [9]. These findings highlight that the optimisation of the DTIS must consider not only the on/off switching of the ventilation but also the modulation of the airflow rate to achieve the desired balance between insulation and conductance performance. In the specific context of the present thesis, the double-leaf brick wall geometry presents an additional complexity compared to laboratory prototypes using homogeneous insulating panels. Brick masonry exhibits inherent thermal mass, and the air cavity between the two leaves will interact with both the inward heat flux from the interior leaf and the outward heat flux from the exterior leaf. The optimisation of airflow through this cavity, and the characterisation of the resulting heat transfer, constitutes the central experimental and analytical objective of this work.

3
METHODOGY

This chapter contains and describes the experimental methodology adopted for this research. It outlines the preconditions established prior to testing, the configuration of the measurement equipment, and the procedures followed to ensure the accuracy and repeatability of the produced results. It should be noted that certain aspects of the methodology remained subject to refinement throughout the course of the research, as familiarity with the equipment increased and practical experience informed adjustments to the experimental setup.

A multitude of different configurations was tested, with variations introduced in the positioning of the inlet fans, the extent to which the upper opening was blocked using insulation material, and the size of the exhaust area employed in each case.

The main objective of this research is to test different geometrical setups and find an optimal configuration to enhance air flow within the air cavity of a double-leaf wall retrofitted with a DTIS. As mentioned in chapter 2.2.2 the case study is a proof-of-concept wall available in the lab. The rear side of the wall has a climatic chamber allowing for variable climate control. During all the test carried out, the climatic chamber is set for a constant temperature of 40 °C and a relative humidity of 60%.

3.1 WALL AND CLIMATIC CHAMBER

The DTIS wall consisted of a double brick leaf construction, with overall dimensions of 1900 mm in width and 1900 mm in height and a total wall thickness of 403 mm. On the exterior side, the wall incorporated an insulation panel with a thickness of 60 mm, finished with an acrylic based coating of 3 mm in thickness (Figure 5). The wall assembly includes two openings, each consisting of a horizontal strip measuring 1900 mm in width and 100 mm in height.

For the purposes of testing, these openings were partially blocked using insulation material. With specific extent of blockage varying according to the configuration that is being examined. Along the bottom side of the wall, several fan pairs were installed to introduce ambient air into the air cavity. This air subsequently travelled upward through the wall cavity, with openings positioned on the top side of the wall allowing the resulting exhaust air to escape.

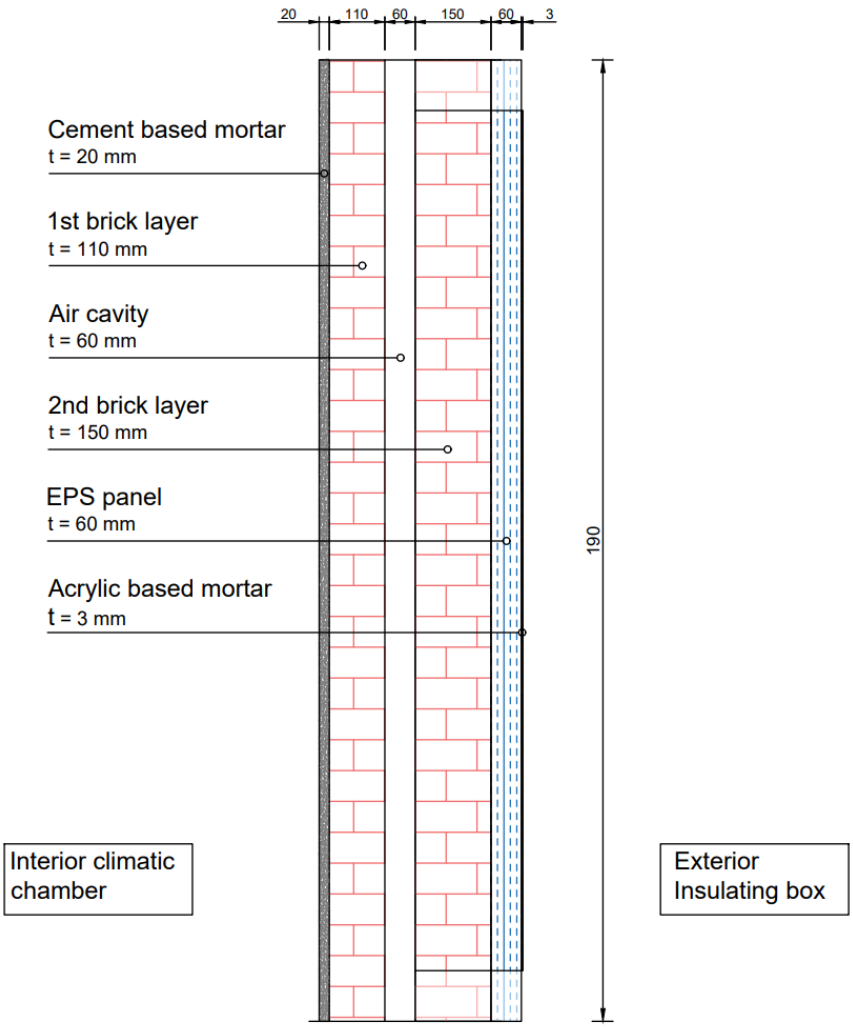


Figure 5: Cross-section of the DTIS wall

To establish a reliable baseline, the tests were conducted with the climatic chamber mainly active, thereby minimising variability when cross comparing the results. One experiment has been conducted with the chamber inactive to measure the influence of the stack effect.



Figure 6: Image of the DTIS wall with the openings sealed

3.2 TRACER GAS MONITORING

The experimental setup centres on a double-leaf brick wall specimen with an integrated climatic chamber, which enables precise regulation of the temperature conditions on one side of the wall. To assess the ventilation rate of the air cavity, carbon dioxide (CO_2) is introduced from a pressurised canister to serve as the tracer gas. The concentration of CO_2 within the cavity is then monitored continuously using a series of data loggers distributed across the cavity volume. In addition, a system of fans and insulating elements is employed to vary the ventilation configuration of the cavity, allowing different airflow conditions to be tested systematically to identify the most thermally effective arrangement. Each of these components is described in further detail in the sections that follow.

3.2.1 Data Logger Configuration and Calibration

As established in the state of the art, CO_2 is used as the tracer gas for airflow characterisation in accordance with the concentration decay method defined in ISO 12569:2017 [15]. The CO_2 concentration within the wall cavity is measured using data loggers capable of recording the concentration in parts per million (ppm) at one second intervals. Prior deployment in the wall cavity all the loggers were calibrated under controlled conditions to ensure consistency and measurement accuracy. The CO2 sensor within the datalogger has a margin of error of ± 50 ppm with ± 5% reading at a temperature of 25°C. These values are considered for future diagnostics.

A total of 12 data loggers were available for use in the laboratory. Calibration was carried out by placing all loggers simultaneously inside an airtight enclosure of known internal volume, fitted with a small aperture to permit a very limited degree of natural air exchange (Figure 7). The enclosure was sealed and a brief injection of CO_2 was administered, after which the experiment was allowed to run over a weekend period with the laboratory unoccupied. This ensured that no external sources of CO_2, such as the respiration of laboratory personnel, influenced the measurements during the decay period.



Figure 7: Enclosure for logger configuration

The gradual decrease in CO_2 concentration over time also referred to as the concentration decay period, was recorded continuously by each logger (Figure 8). The resulting decay data were used to determine the air change rate of the enclosure using Equation 1.1, which is derived from the logarithmic transformation of the exponential decay curve. This linearisation allows the decay rate constant to be extracted through linear regression, from which the air changes per hour (ACH) and the associated volumetric airflow rate are calculated.

The natural logarithm of C(t) was plotted against time, and linear regression was applied to determine the trendline for each dataset. The slope of the resulting trendline corresponds to the hourly air exchange rate.

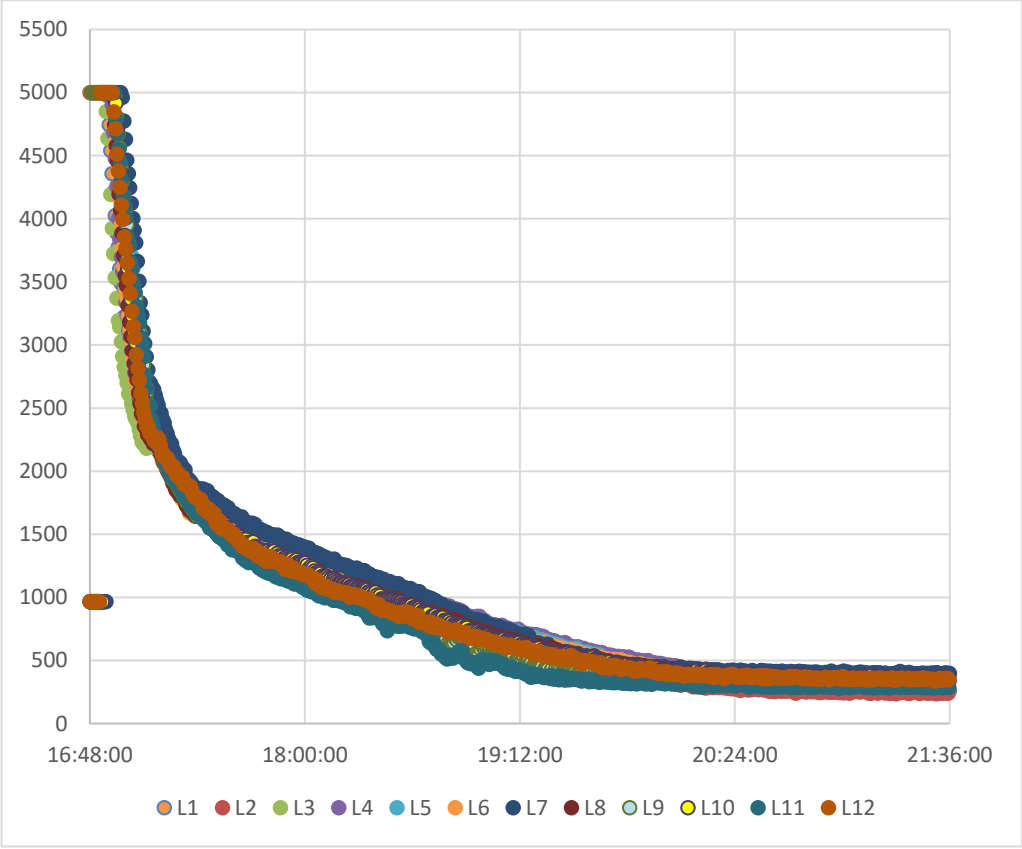


Figure 8: Plot of the natural CO2 decay for each logger

Following the test, the ACH was calculated from the decay curve of each individual logger. Based on these results, a selection process was carried out to identify the loggers exhibiting the least deviation from one another, and these were subsequently selected for use in the main experiments. Figure 9 shows the box-plot representation of the individual ACH values, including the clusters of the "best suitable" and "least suitable" loggers when compared to the baseline value. Loggers with ACH values between 0.53 h^{-1} and 0.56 h^{-1} were considered the most accurate and were therefore selected for use in the subsequent experiments.

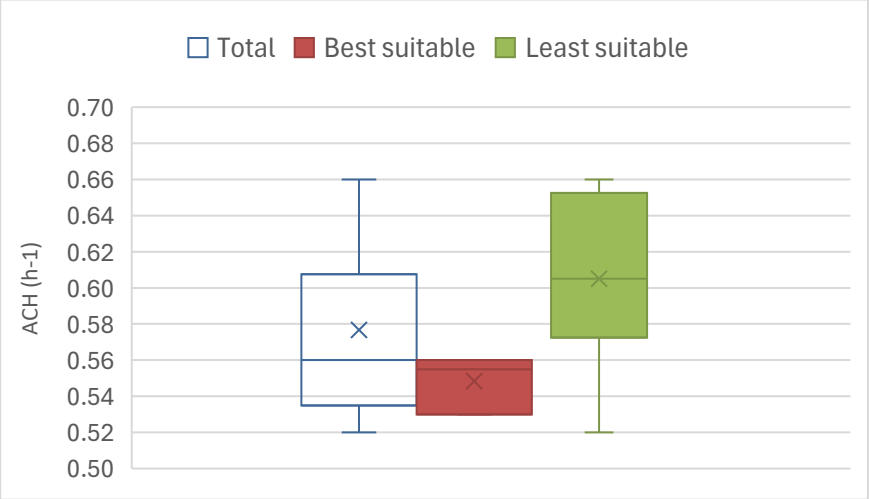


Figure 9: Suitability ranges of the loggers in ACH (h-1)

Table 1 shows the ranking of the loggers with the respective calculated ACH. After this procedure, the loggers positioned within the wall cavity were labelled as L10, L6, L8, L12, L5, and L3; and loggers L11 and L7 were placed at the inlet and outlet, respectively, while L4 was used to measure the ambient CO_2 concentration (in the lab).

Table 1: Ranking of the loggers

Best suitable		**Least suitable**	
Logger	**ACH**	**Logger**	**ACH**
L10	0.56	L1	0.60
L6	0.53	L11	0.66
L8	0.53	L4	0.52
L12	0.56	L2	0.61
L5	0.56	L7	0.59
L3	0.55	L9	0.65
Ave	0.55	**Ave**	0.61
SD	0.013	**SD**	0.046

3.2.2 Tracer gas injection

It is essential that the inlet and outlet areas requiring insulation exhibited a high degree of air tightness to achieve accurate test measurements. Therefore, ensuring that minimal to no tracer gas escaped into surrounding areas of the wall assembly. Insulation material with a thickness of 100 mm was used to block the openings for each selected experimental configuration.

Each insulation panel was carefully measured and cut with a slight taper along the top edge allowing it to function as a wedge once placed. This reasoning ensured that the insulating material fitted snugly within the wall cavity, minimising the presence of gaps through which air could pass. To further guarantee maximum airtightness, the edges of each insulation panel were sealed using gaffer tape. This provides an additional barrier against unwanted air infiltration or exfiltration.

On the upper level of the wall two tubes with a diameter of 3 mm were installed to facilitate the injection of the tracer gas. These tubes were routed through two relief holes cut into the insulation. This allows them to enter the wall cavity and inject the gas at consistent locations. This arrangement ensured that the injection process remained repeatable across the various experimental configurations. The CO_2 gas required for the tracer gas method was supplied from a 200 litre canister, fitted with a pressure limiter set to 1 Bar. This mechanism enabled a more controlled injection flow of CO_2 into the wall cavity.



Figure 10: CO_2 gas cannister and DTIS wall setup

3.3 EXPERIMENTAL SETUP

3.3.1 Placement of the loggers

As previously outlined in Chapter 3.2, the individual CO_2 loggers were ranked according to their measured accuracy. This resulted in a clear distinction between the most and least suitable loggers for the use in the main experimental campaign. Given the importance of measurement precision for the reliability for the ACH calculations: it was determined that only the most accurate loggers would be used within the wall cavity itself. This selective placement strategy was considered essential in ensuring that the decay measurements obtained during testing would be as accurate and reliable as possible.

In accordance with this approach, logger L11 was positioned at the inlet of the wall cavity, while logger L7 was placed at the outlet. These two locations were considered important, as they allowed the CO_2 concentration to be monitored at the points where air entered and exited the cavity. Therefore, providing valuable insight into the airflow behaviour across the full length of the wall. In addition to the loggers placed within the cavity itself, logger L4 was positioned outside the wall assembly, where it served to measure the ambient CO_2 concentration of the surrounding air. This ambient measurement was considered necessary to provide a reliable reference value against which the CO_2 concentrations recorded within the wall cavity could be compared. A schematic overview illustrating the placement of the individual loggers is presented in Figure 11.

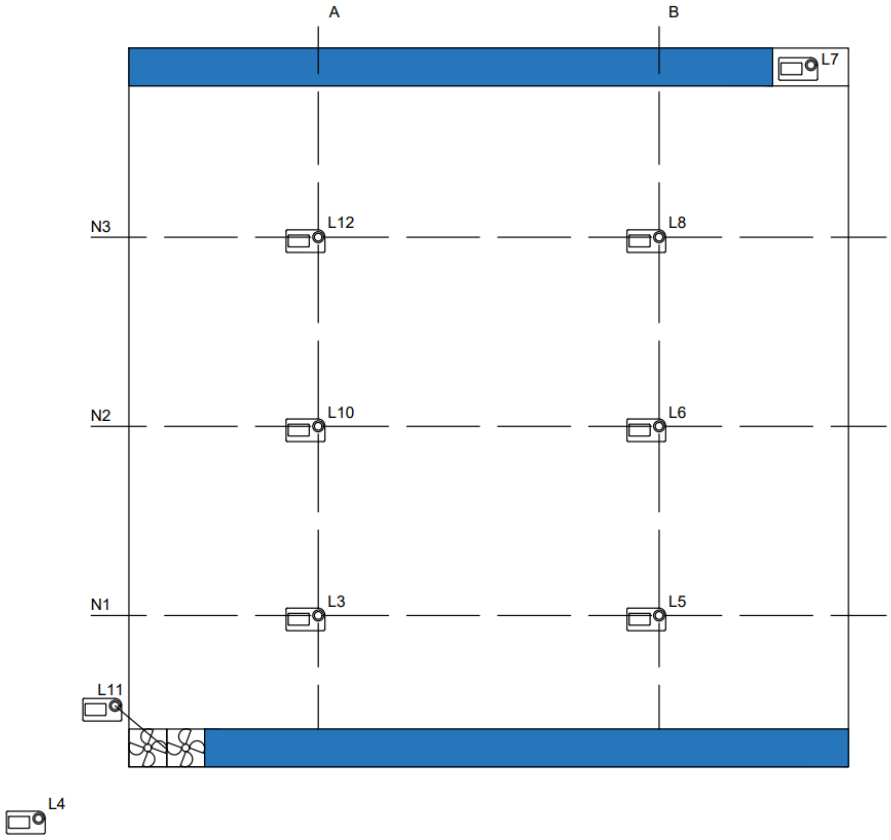


Figure 11: Placement of the loggers

For the physical installation of the loggers, each logger was attached to a carabiner with a use of fishing line. This method was chosen specifically for its ability to provide a robust and reliable connection while remaining unobtrusive within the reduced space of the wall cavity. To secure this system, two ring anchors were fixed to the upper side of the wall, providing secure attachment points to which the carabiners could be connected. Once it was attached, the loggers were carefully lowered into the wall cavity where they remained suspended by the fishing line for the duration of the entire experiment.

This method of installation was deliberately chosen for several practical reasons. The first reason is that it allowed for the loggers to be positioned within the wall cavity while occupying a minimal amount of space, thereby avoiding any unnecessary obstruction of the airflow being measured. Second, the use of a carabiner and fishing line method provided a quick and straightforward means of securing the loggers in place, considerably simplifying the setup process ahead of each experimental run. Once the experiment had been completed, the loggers could similarly be raised and removed from within the wall cavity with relative ease, allowing the recorded data to be promptly extracted and prepared for subsequent analysis.

3.3.2 Fans wiring

The design and realisation of the electrical circuit for the fan system required careful consideration given the considerable degree of variability inherent in the range of configurations that were tested. Added the frequently changing positions in which the fans were required to be placed within the wall cavity needed to be taken in account for. Given that the experimental setup demanded a high degree of variability, it was necessary to design a wiring system that could accommodate these varying spatial and operational requirements without compromising the reliability or safety of the electrical connections.

For this reason, each fan group was connected using a dedicated cable with a length of at least 2000 mm in length. This cable length was selected to provide sufficient flexibility. This allowed for the position of each fan group to be adjusted freely within the wall cavity according to the specific demands of a given configuration. Without placing any strain on the electrical connections or requiring the cables to be extended or modified between tests. Added, the fans within each group were physically attached to one another, ensuring that they remained in a fixed and stable relative position throughout the duration of testing. Thereby minimising the risk of unintended movement or misalignment once installed within the cavity.

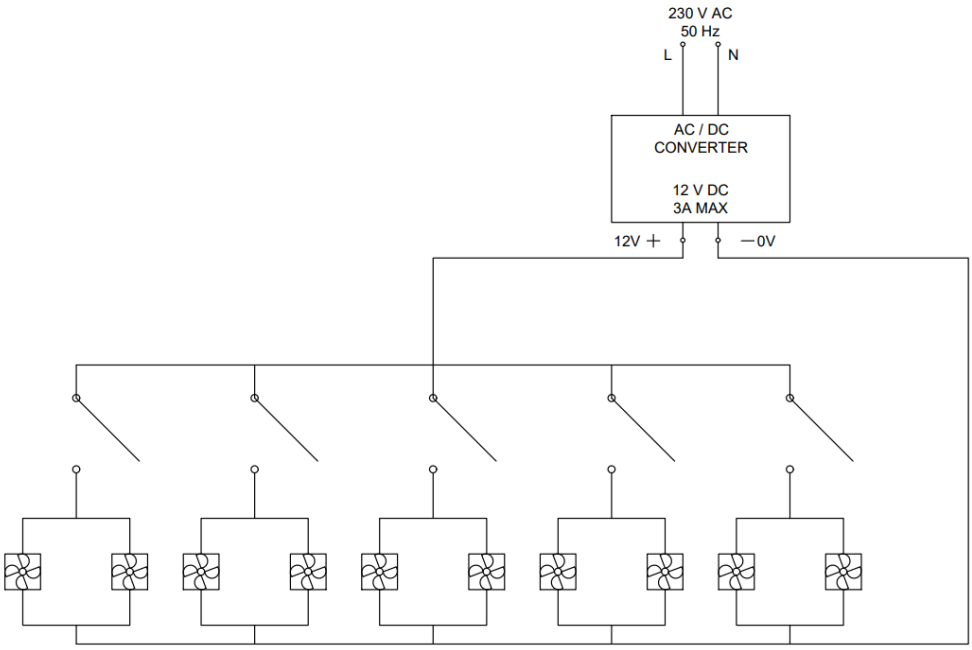


Figure 12: Wiring diagram

In terms of its electrical characteristics, the fan system was designed to operate on 12 volts of DC (direct current). The mains power supply available for the experimental setup provided an AC (alternating current) of 230 volts, it was necessary to incorporate an alternating current to direct current converter into the circuit. This allowed for the mains supply to be stepped down and converted to the 12 volts required for proper operation of the fans. Regarding the wiring arrangement itself, the fans were wired together in groups of two, with the resulting fan groups subsequently wired in parallel with one another as seen in Figure 12.

This approach to wiring the fan system offered several practical advantages within the context of the experimental setup. It allowed each individual fan group to be switched on or off entirely independently of the others. Therefore providing a high degree of control over which fans were active at any given time. Furthermore, because the fan groups were wired in parallel and connected using sufficiently long flexible cabling each group could be repositioned freely within the wall cavity as required.

3.3.3 Configurations

In total, six distinct configurations were tested to evaluate the effect of varying fan quantity and inlet and exhaust opening size on the resulting airflow within the wall cavity as seen in figure 13. The first configuration made use of a single fan group, consisting of two fans, and served as a baseline against which the subsequent, more complex configurations could be compared. Building on this baseline, three further configurations were tested using two fan groups, amounting to four fans in total, with each of these three configurations differing from one another in terms of the size of the inlet and exhaust openings employed. This approach allowed the effect of opening size to be evaluated independently of fan quantity, while keeping the number of active fans constant across the three configurations. Finally, two additional configurations were tested using three fan groups, corresponding to a total of six fans, again with variations introduced in the opening sizes between the two configurations.

The decision to limit the maximum number of fans tested to six was based on observations made during the testing phase of the research. It was found that increasing the number of active fans beyond six did not result in a meaningful or proportionate increase in the resulting airflow within the wall cavity.

For each of the six configurations tested, particular care was taken to ensure that the sides of the insulation material used to block off the unused openings were sealed as thoroughly as possible using gaffer tape. This measure was implemented to achieve as airtight a seal as possible around the edges of each insulation panel, thereby minimising the extent to which CO_2 could escape through the sides of the insulation during testing. Ensuring a consistently high standard of sealing across all configurations was considered essential in maintaining the reliability and comparability of the results obtained, as any inconsistency in sealing quality between configurations could otherwise have introduced a confounding source of variability into the measured airflow and ACH values.

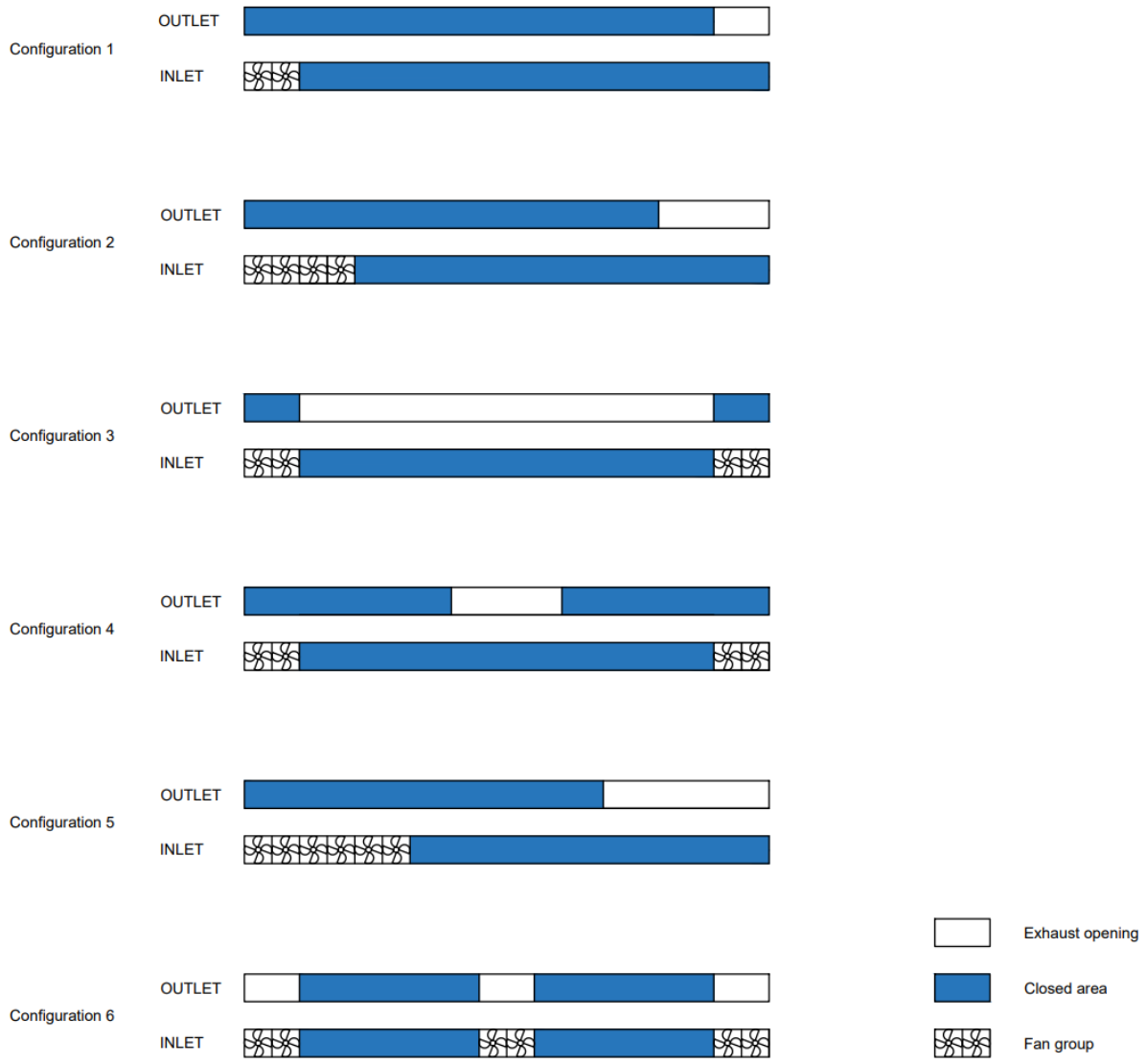


Figure 13: Configurations

3.4 TEST PROCEDURES

The experimental procedure was composed of three major steps: injection, settlement, and decay as seen in figure 14. These three steps were repeated a minimum of five times per experiment to ensure a sufficient degree of repeatability and to allow for a reliable statistical assessment of the results obtained. Each of these individual steps is explained in greater detail in the following sections.

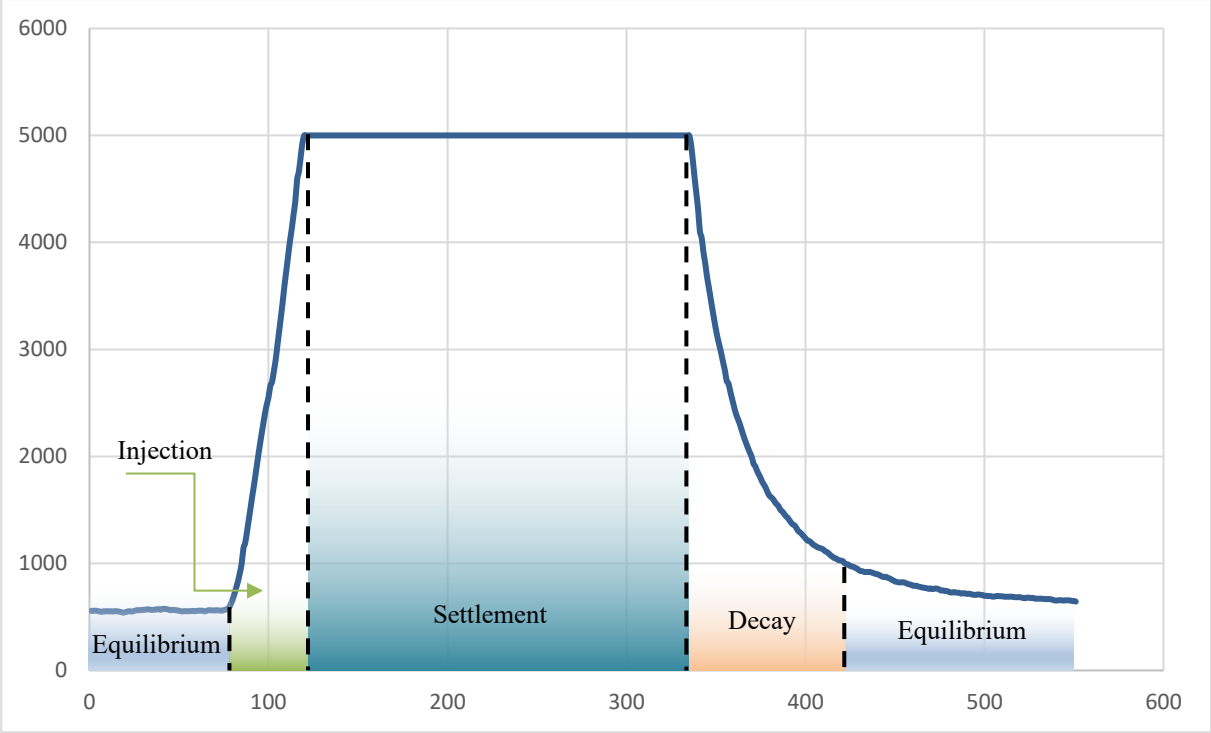


Figure 14: Phases of the decay experiment

3.4.1 Injection

Injection constituted the first phase of the experimental procedure. Prior to the start of each experiment, the climatic chamber was operated for a minimum period of 8 hours at a temperature of 40 °C and a relative humidity of 60%, thereby ensuring that stable and representative climatic conditions had been established within the chamber before testing commenced. During this phase, all openings within the wall assembly, including the fan inlets, were sealed using custom-fitted pieces of insulation, with the edges additionally taped to further improve the seal. As a result of these measures, the wall cavity was maintained in a fully closed state, allowing only a minimal exchange of ambient air with the surrounding environment.

Once this closed state had been established, CO_2 was injected into the wall cavity using the tubes connected to the gas canister, with the injection process carried out in such a way as to minimise any escape of air from the cavity. Owing to the high pressure maintained within the canister, only a relatively short burst of gas was required in order to fully saturate the air within the cavity with CO_2.

3.4.2 Settlement

Following the injection of the tracer gas, a period of time was required to allow the air within the wall cavity to settle and distribute evenly throughout the available volume. Given that the injection tubes were positioned at the upper part of the cavity and that CO_2 has a higher density than oxygen, the gas tended to settle downward over time. Injecting the CO_2 from the upper side of the cavity therefore promoted a more even distribution over the entire cavity volume. A certain amount of time was required for this distribution process to take place. As previously noted, the loggers used in this study had a maximum measuring range of 5000 ppm. To obtain the most accurate possible measurements, it was considered essential that the wall cavity be saturated to a sufficient degree that all loggers recorded values above this threshold. Should any individual logger fail to register a sufficiently high value, the resulting decay calculation for that test would be rendered invalid.

Over the course of the experimental campaign, it was determined that a settlement window of between 3 and 5 minutes represented the optimal duration for this phase. Where the settlement period was shorter than 3 minutes, the loggers were generally found not to reach a measurement of at least 5000 ppm. Conversely, where the settlement period exceeded 5 minutes, a degree of air leakage was observed to occur, resulting in a gradual decline in CO_2 concentration and, consequently, measured values falling below the required threshold of 5000 ppm.

3.4.3 Decay

The third and final step of the experimental procedure was the decay phase. Once a sufficient period of time had elapsed following the settlement phase, the pieces of insulation blocking the various openings were removed, and the fans were switched on immediately afterward. Upon activation, the fans introduced ambient air with a CO_2 concentration of approximately 400 ppm into the cavity, while the CO_2 rich air present within the cavity was simultaneously extracted from the upper side of the wall. In a manner like that employed during the logger calibration procedure, the time required for the CO_2 concentration to decay to a specified target value was subsequently used to calculate the corresponding ACH value. During the preliminary phase of the research, a target value of 1000 ppm was used for this purpose; this value was later revised to improve the overall accuracy of the resulting ACH calculations.

It should be noted that precisely determining the CO_2 concentration values in real time during testing was not a straightforward task, given that the loggers were positioned deep within the wall cavity and therefore not directly visible or easily accessible during the course of the experiment. In order to accurately time the various steps of the procedure despite this limitation, a dedicated solution was developed, the details of which are explained further in the following section.

3.4.4 Monitoring Procedures

Throughout the course of each experiment, the loggers were used to monitor the CO_2 concentration at a measurement interval of 1 second. By connecting the loggers to a computer by means of an extended USB cable, it was possible to observe the real time CO_2 concentration values as the experiment progressed. This approach considerably improved both the efficiency and the accuracy with which the experiments could be conducted, since accurately gauging the CO_2 concentration in parts per million would not otherwise have been practically feasible.

The logger selected for real-time monitoring during testing was logger L7. Given that this logger was positioned on the upper side of the wall cavity, it was expected to be the logger most delayed in registering the target CO_2 concentration, since, as previously discussed: CO_2 tends to sink downward within the cavity owing to its higher density relative to ambient air. Consequently, it was reasoned that once the highest-positioned logger recorded a sufficiently high concentration value, the remaining loggers positioned lower within the cavity could reasonably be assumed to have reached sufficient concentration levels as well.

4
RESULTS

4.1 EXPERIMENTS OVERVIEW

Once all pretest preparations had been concluded, the experiments could be initialised. This chapter presents the results of ten tests conducted under a range of different configurations and experimental setups, each designed to investigate the effect of varying fan quantity, fan positioning, inlet and exhaust opening size on the resulting airflow within the wall cavity. For each experiment, the CO2 concentration decay method described in Section 3.2.1 was applied to calculate the corresponding air change rate (ACH), thereby allowing the airflow performance of each configuration to be quantitatively assessed and compared.

The experiments were conducted progressively over the course of the testing campaign, with the methodology and execution being refined as practical experience with the equipment and testing procedure increased. As a result, certain adjustments were introduced between successive experiments, including changes to the number of tracer gas injection bursts performed and the duration of the settlement period, to improve the overall accuracy and consistency of the results obtained. Where such methodological refinements were introduced, or where issues arose during the execution of a particular experiment, these are noted and explained within the corresponding section below.

In addition to varying the fan and opening configurations, a subset of the experiments was conducted with the climatic chamber inactive, to isolate and evaluate the influence of the stack effect on the resulting airflow, independent of the temperature difference normally induced by the chamber. Most experiments, however, were conducted with the climatic chamber active, consistent with the baseline conditions established in Section 3.1, thereby allowing for reliable comparison between the different configuration's tests.

4.1.1 Experiment 1

The initial test was conducted with the climatic chamber inactive. This approach was adopted to verify whether any differences in airflow could be observed between the chamber being active and inactive.

When initially reviewing the data, one of the preconditions established for the analysis was to consider only the portion of the decay curve extending from the first measurement below 5000 ppm to the last measurement above 1000 ppm. Figure 15 presents an example of the regression graphs produced for one measurement, from which the corresponding ACH value was calculated. These two graphs illustrate the regression obtained from the exact same measurement, although analysed under two different sets of preconditions to establish the data.

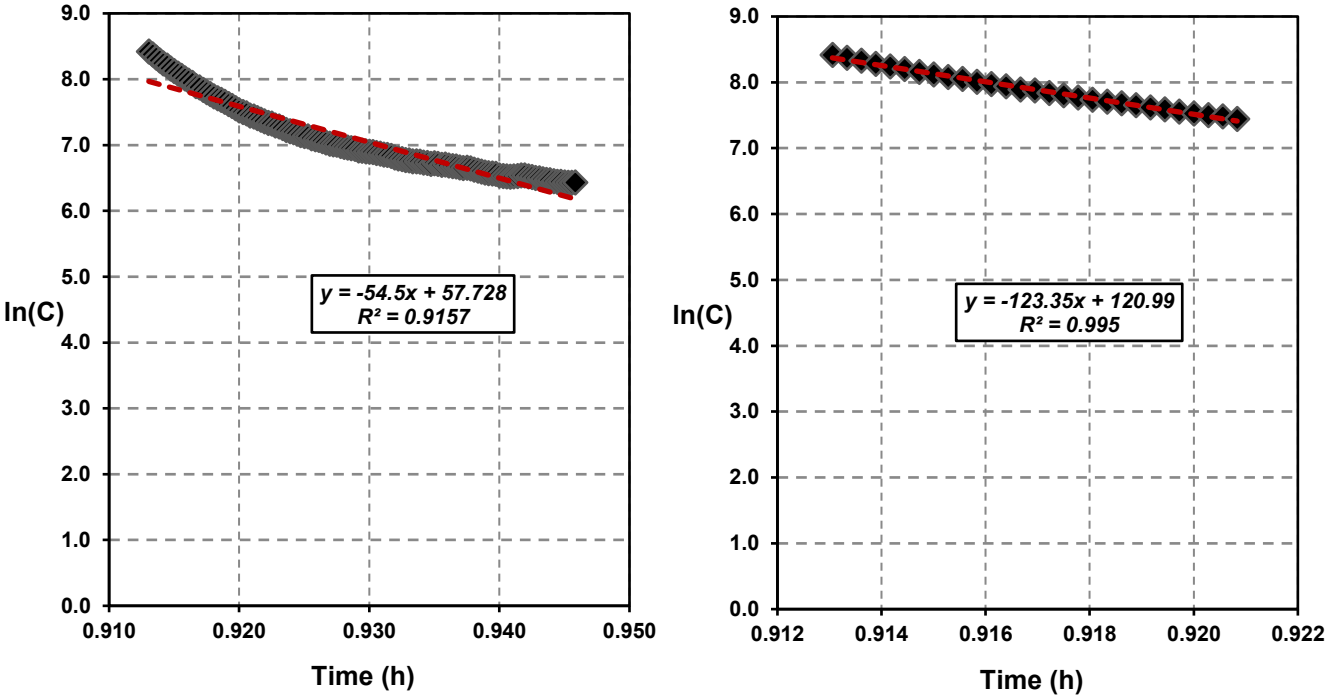


Figure 15: Comparison of regression graphs under different preconditions

A substantial difference in the resulting ACH value was observed between the two approaches as seen in Figure 15: the left-hand graph yielded a plotted ACH of 54.5 h^{-1}, whereas the right-hand graph produced a value of 123.35 h^{-1}, representing an increase of 226%. This considerable discrepancy prompted a closer examination of the underlying methodology used to define the preconditions applied to the data.

The source of this discrepancy was traced to the specific criteria used to select the range of data points included in each regression analysis. The left-hand graph was constructed using the original precondition, in which the full range of data between 5000 ppm and 1000 ppm was included. The right-hand graph, by contrast, was constructed using a revised precondition that accounted for the measurement error margin of the loggers and employed a comparatively shorter time span for the regression.

It was observed that, once the CO2 concentration measured by the loggers dropped below approximately 2000 ppm, the decay curve began to exhibit non-linear behaviour, with the measurements becoming increasingly unstable and occasionally registering a slight increase in ppm relative to the preceding reading. Restricting the regression to a shorter time span and therefore excluding this unstable lower portion of the decay curve, was found to markedly improve the coefficient of determination (R^2) of the resulting regression line.

To establish a well-defined and reproducible precondition for this purpose, rather than selecting the cut-off point arbitrarily, the following criterion was applied:

$$ln(Ct1 - Ct2) \geq ln(50)$$

Where:

- Ct = measurement of the concentration of CO2 in parts per million.

This formula was derived from the fact that the data loggers used in this study carry a stated error margin of ± 50 ppm. Because the ACH is calculated on a logarithmic scale, this error margin likewise needed to be expressed in logarithmic terms to be applied consistently within the regression analysis. Accordingly, where the difference between a given measurement (Ct1) and the subsequent measurement (Ct2) exceeded ln (50), equivalent to approximately 3.912, the corresponding data point was considered to lie within the acceptable error margin and was therefore retained for inclusion in the regression line. Conversely, the first measurement found not to satisfy this condition marked the point at which the data sequence used for the regression was terminated.

As shown in Figure 15, the right-hand graph, constructed in accordance with this revised criterion, produced a markedly improved coefficient of determination ($R^2 = 0.995$), compared with the considerably lower value obtained under the original precondition ($R^2 = 0.9157$). Once this revised criterion had been implemented and applied consistently across the full dataset, the accuracy of the previously calculated ACH values improved significantly, with all resulting R^2 values subsequently exceeding 0.99.

It is worth noting that, prior to the implementation of this revised precondition, the ACH values obtained between individual measurement cycles fluctuated considerably, making reliable comparison between the various tested configurations extremely difficult. This fluctuation was, in fact, the underlying reason for the repetition of Experiments 5 and 6, as the ACH values initially calculated for these two experiments produced contradictory outcomes that could not be reliably interpreted under the original analytical approach.

With having these preconditions established the results of the experiments can be represented. The experiment was carried out using the first configuration (Figure 16), comprising two fans positioned on the left side of the wall, with an opening of 200 x 100 mm located on the top right side of the wall. This opening was sized to match the area occupied by the fans.

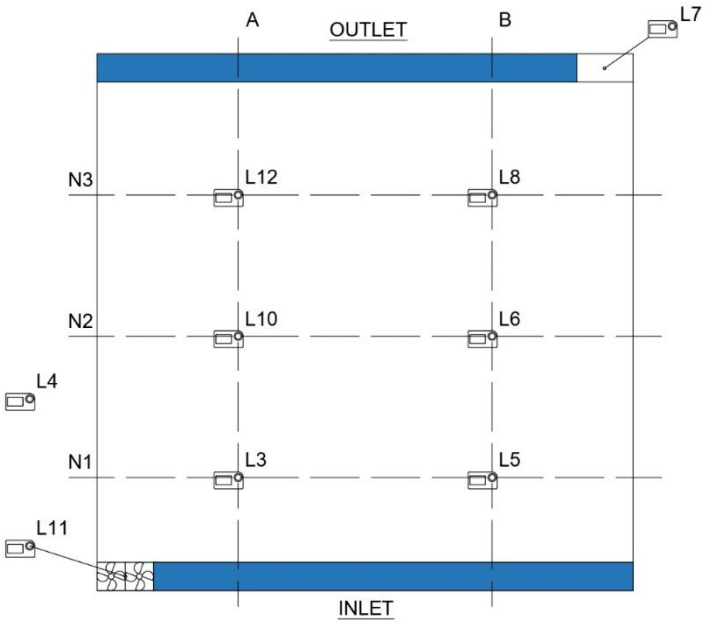


Figure 16: Configuration 1

Table 2 presents the calculated hourly exchange rate of each individual logger. The experiments contained a total of three CO2 bursts.

Table 2: Results of experiment 1 in ACH (h-1)

Experiment 1	**L11**	**L3**	**L10**	**L12**	**L5**	**L6**	**L8**	**L7**
ACH 1	292.0	92.0	20.0	73.0	167.0	145.0	197.0	226.0
ACH 2	276.0	107.0	59.0	114.0	150.0	132.0	167.0	185.0
ACH 3	258.0	104.0	66.0	109.0	139.0	131.0	165.0	175.0
AVG	275.3	101.0	48.3	98.7	152.0	136.0	176.3	195.3

4.1.2 Experiment 2

For this experiment, the climatic chamber was switched on, while the configuration remained identical to that used in Experiment 1. Owing to significant errors in the execution of the experiment, the resulting logger data had to be rejected. Specifically, logger L5 was found to have a cable wrapped around its sensor head, which obstructed the CO2 flow and consequently resulted in delayed measurements.

In addition, the settlement time had been reduced to speed up the overall testing process; however, this meant that the loggers did not have sufficient time to level out, and no accurate readings could therefore be obtained. As a result of these combined issues, this experiment was repeated at a later stage, and the values of this experiment were disregarded.

4.1.3 Experiment 3

Following the acquisition of further insight into the methodology and subsequent improvements to the execution of the tests, the same configuration (Configuration 1, Figure 16) was set up again, this time with the climatic chamber active. This experiment was considered particularly important, as it represented the first successful test conducted following the issues encountered in Experiment 2, thereby providing the initial reliable dataset against which subsequent experiments could be compared.

To further improve measurement accuracy, a minimum of five injection bursts were conducted for this experiment, rather than the three used previously. This adjustment was made in direct response to the settlement-related issues identified in Experiment 2, with the additional bursts intended to improve the overall consistency and comparability of the results obtained across tests.

Table 3: Results of experiment 3 in ACH (h-1)

Experiment 3	**L11**	**L3**	**L10**	**L12**	**L5**	**L6**	**L8**	**L7**
ACH 1	332.0	176.0	70.0	127.0	76.0	131.0	204.0	224.0
ACH 2	383.0	155.0	74.0	129.0	152.0	154.0	209.0	112.0
ACH 3	388.0	156.0	70.0	131.0	141.0	154.0	220.0	205.0
ACH 4	418.0	162.0	78.0	131.0	152.0	148.0	223.0	203.0
ACH 5	389.0	149.0	61.0	108.0	143.0	136.0	206.0	190.0
AVG	382.0	159.6	70.6	125.2	132.8	144.6	212.4	186.8

4.1.4 Experiment 4

This test was conducted using the second configuration, comprising four fans arranged as an inlet, together with a single outlet opening measuring 400 x 100 mm. This configuration represented the first step beyond the two-fan arrangement tested in the preceding experiments, allowing the effect of an increased fan quantity on the resulting airflow to be evaluated for the first time within this experimental campaign (Configuration 2, Figure 17). The experiment was carried out shortly after Experiment 3, meaning that the loggers remained in the same physical positions and that ambient temperature and CO2 concentration levels were relatively consistent between the two tests.

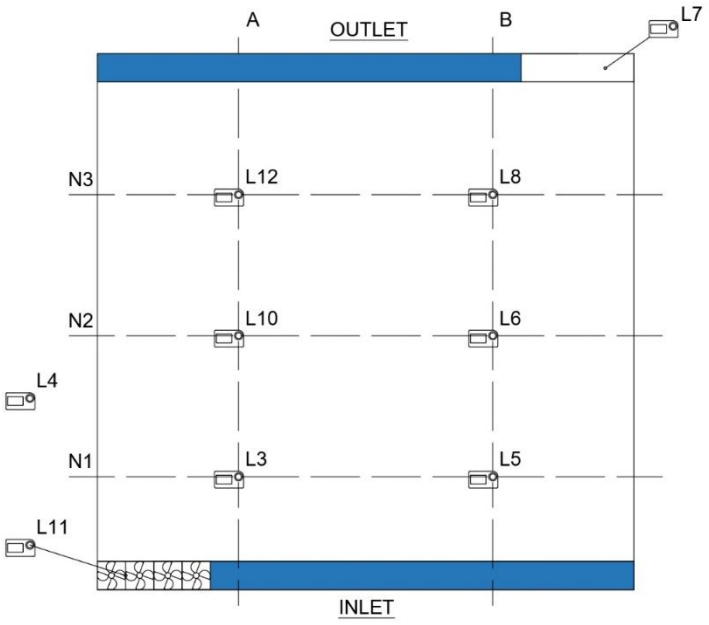


Figure 17: Configuration 2

The insulation material was cut to the appropriate dimensions required for this configuration, and the loggers were positioned accordingly, in line with the placement procedure described in Section 3.3.1. Attention was paid to ensuring that the edges of the insulation panels remained tightly sealed following this adjustment, given that any reduction in airtightness at this stage could have introduced additional variability into the resulting measurements.

Table 4 presents the calculated hourly exchange rate for each individual logger.

Table 4: Results of experiment 4 in ACH (h-1)

Experiment 4	**L11**	**L3**	**L10**	**L12**	**L5**	**L6**	**L8**	**L7**
ACH 1	363.0	226.0	97.0	220.0	160.0	150.0	272.0	287.0
ACH 2	351.0	228.0	79.0	181.0	147.0	135.0	262.0	258.0
ACH 3	342.0	203.0	73.0	157.0	136.0	128.0	236.0	221.0
ACH 4	375.0	201.0	76.0	195.0	135.0	134.0	251.0	232.0
ACH 5	374.0	204.0	76.0	190.0	140.0	132.0	257.0	227.0
AVG	361.0	212.4	80.2	188.6	143.6	135.8	255.6	245.0

4.1.5 Experiment 5

Experiment 5 was conducted with Configuration 3, which similarly employed four fans in total; however, in this case, each pair of fans was positioned on either side of the chamber, with the insulation material located centrally between the two fan groups (Configuration 3, Figure 18).

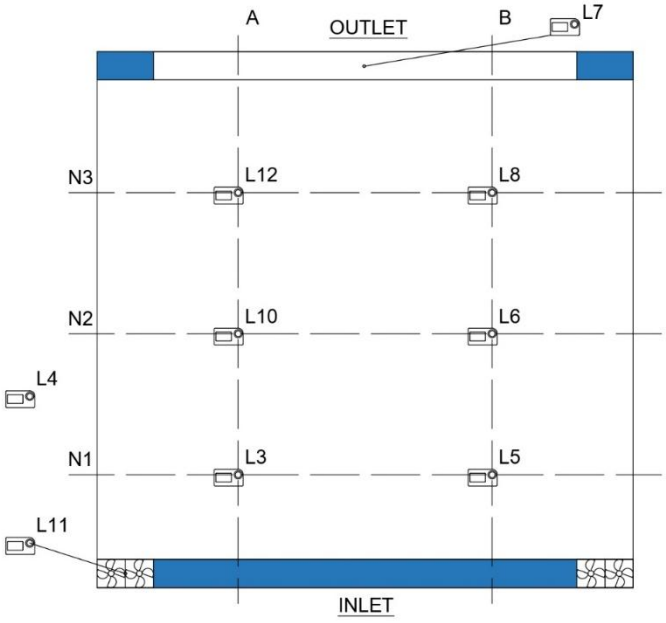


Figure 18: Configuration 3

The opening on the upper side of the wall measured 1500 x 100 mm, meaning that the blocked sections consisted of two areas measuring 200 x 100 mm each. Whereas the previous experiments had employed openings equal in area to that occupied by the fans, this experiment instead adopted the opposite approach: the inlet area at the bottom of the wall was matched in size to the blocked area at the top. The experiment was subsequently conducted using this considerably wider opening configuration for future comparison of the effect of the outlet area.

Table 5 presents the calculated hourly exchange rate for each individual logger.

Table 5: Results of experiment 5 in ACH (h-1)

Experiment 5	L11	L3	L10	L12	L5	L6	L8	L7
ACH 1	572.0	172.0	89.0	160.0	181.0	138.0	144.0	116.0
ACH 2	542.0	152.0	82.0	142.0	166.0	134.0	135.0	115.0
ACH 3	568.0	170.0	102.0	177.0	188.0	142.0	157.0	116.0
ACH 4	556.0	168.0	109.0	177.0	180.0	146.0	146.0	113.0
ACH 5	545.0	168.0	93.0	172.0	176.0	139.0	151.0	112.0
AVG	556.6	166.0	95.0	165.6	178.2	139.8	146.6	114.4

4.1.6 Experiment 6

This experiment was conducted using the same inlet configuration as employed in Experiment 5, comprising four fans arranged in two groups positioned on either side of the chamber, with the insulation material located centrally between them (Configuration 4, Figure 19). In contrast to Experiment 5, the outlet area in this case was matched to the inlet area, consistent with the approach adopted in Experiments 1 through 4.

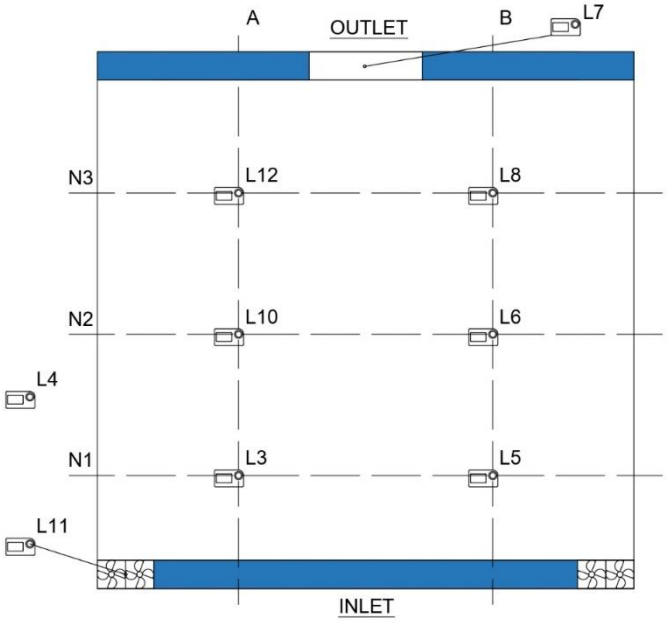


Figure 19: Configuration 4

By maintaining an identical inlet setup across both experiments, it was possible to isolate the specific effect of outlet opening size on the resulting airflow within the wall cavity. This experiment was conducted shortly after Experiment 5, ensuring that the loggers remained in their established positions and that ambient conditions within the laboratory remained largely consistent between the two tests for minimizing variability and maximizing the accuracy of the outlet comparison.

Table 6 presents the calculated hourly exchange rate for each individual logger.

Table 6: Results of experiment 6 in ACH (h-1)

Experiment 6	**L11**	**L3**	**L10**	**L12**	**L5**	**L6**	**L8**	**L7**
ACH 1	433.0	147.0	40.0	99.0	103.0	114.0	189.0	198.0
ACH 2	415.0	137.0	36.0	81.0	94.0	100.0	147.0	181.0
ACH 3	377.0	138.0	40.0	87.0	127.0	107.0	156.0	188.0
ACH 4	341.0	134.0	41.0	87.0	122.0	105.0	147.0	182.0
ACH 5	362.0	137.0	41.0	79.0	111.0	99.0	137.0	163.0
AVG	385.6	138.6	39.6	86.6	111.4	105	155.2	182.4

4.1.7 Experiment 7

Experiment 7 represented the first configuration in which six fans were introduced (Configuration 5, Figure 20). As in Experiments 1 through 4, the outlet area was set equal to the inlet area, allowing this expanded fan arrangement to be evaluated under conditions comparable to the earlier tests. This configuration was of particular interest, as it represented the first step beyond the four-fan arrangements tested in the preceding experiments, providing an initial indication of whether a further increase in fan quantity would yield a proportionate improvement in the resulting airflow within the wall cavity.

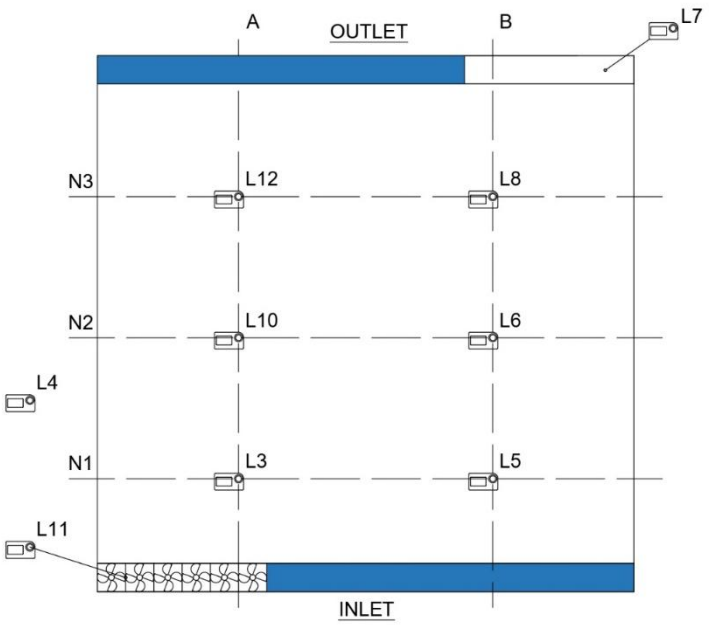


Figure 20: Configuration 5

As indicated in orange in the accompanying table, the sensor of logger L5 was found to be wrapped around a cable and consequently partially obstructed. This issue was identified upon removal of the loggers following the experiment, as logger L5 proved considerably more difficult to extract than the remaining loggers. Consequently, the data recorded by this logger for the present experiment were disregarded and excluded from subsequent data analysis.

Table 7 presents the calculated hourly exchange rate for each individual logger.

Table 7: Results of experiment 7 in ACH (h-1)

Experiment 7	L11	L3	L10	L12	L5	L6	L8	L7
ACH1	425.0	220.0	91.0	95.0	41.0	125.0	246.0	351.0
ACH2	421.0	224.0	87.0	85.0	39.0	120.0	243.0	278.0
ACH3	409.0	219.0	89.0	94.0	30.0	124.0	247.0	285.0
ACH4	413.0	215.0	96.0	93.0	35.0	126.0	250.0	280.0
ACH5	425.0	234.0	100.0	99.0	25.0	129.0	267.0	316.0
AVG	418.6	222.4	92.6	93.2	34.0	124.8	250.6	302

4.1.8 Experiment 8

Following analysis of the results obtained from Experiments 5 and 6, it was decided that both experiments should be repeated, with the two repeated tests conducted consecutively to minimise variability arising from fluctuations in ambient conditions between test days. This experiment was carried out using the same configuration as Experiment 6 (Configuration 4, Figure 20), comprising four fans and a small outlet opening measuring 400 x 100 mm on the top side of the wall.

Particular care was taken during the setup of this repeated experiment to ensure that the insulation panels were fitted and sealed with the same degree of precision as in the original test, and that the loggers were returned to their previously established positions within the cavity, in order to maintain consistency between the original and repeated datasets.

Table 8 presents the calculated hourly exchange rate for each individual logger.

Table 8: Results of experiment 8 in ACH (h-1)

Experiment 8	**L11**	**L3**	**L10**	**L12**	**L5**	**L6**	**L8**	**L7**
ACH1	405.0	108.0	73.0	102.0	69.0	100.0	162.0	161.0
ACH2	373.0	97.0	77.0	94.0	70.0	98.0	144.0	129.0
ACH3	418.0	94.0	79.0	123.0	80.0	102.0	178.0	153.0
ACH4	415.0	100.0	77.0	123.0	77.0	101.0	177.0	153.0
ACH5	359.0	116.0	82.0	130.0	74.0	103.0	174.0	154.0
AVG	394.0	103.0	77.6	114.4	74.0	100.8	167.0	150.0

4.1.9 Experiment 9

This experiment was conducted using the same configuration as Experiment 5 (Configuration 3, Figure 18), comprising four fans and a wide outlet opening measuring 1500 x 100 mm. As with Experiment 8, this test formed part of the repeated pairing of Experiments 5 and 6 and was carried out immediately following Experiment 8 to ensure both repeated tests were conducted under closely comparable ambient conditions.

Conducting Experiments 8 and 9 consecutively was considered particularly important given that these two experiments were intended to be directly compared with one another to evaluate the effect of outlet opening size, while all other variables remained constant. By minimising the time elapsed between the two tests, the potential influence of external factors was reduced, thereby improving the reliability of the resulting comparison.

Table 9 presents the calculated hourly exchange rate for each individual logger.

Table 9: Results of experiment 9 in ACH (h-1)

Experiment 9	**L11**	**L3**	**L10**	**L12**	**L5**	**L6**	**L8**	**L7**
ACH1	417.0	116.0	94.0	145.0	147.0	121.0	208.0	77.0
ACH2	417.0	123.0	94.0	152.0	159.0	124.0	216.0	86.0
ACH3	391.0	126.0	108.0	152.0	158.0	133.0	210.0	121.0
ACH4	413.0	114.0	82.0	133.0	143.0	115.0	207.0	82.0
ACH5	393.0	124.0	104.0	153.0	165.0	130.0	215.0	83.0
AVG	406.2	120.6	96.4	147.0	154.4	124.6	211.2	89.8

4.1.10 Experiment 10

To conclude the experimental campaign, a final configuration featuring a distinct setup relative to the previous configurations was tested. As in Experiment 7, six fans were employed; however, in this case, one fan group was positioned on either side of the wall, with an additional fan group placed centrally within the cavity (Configuration 6, Figure 21).

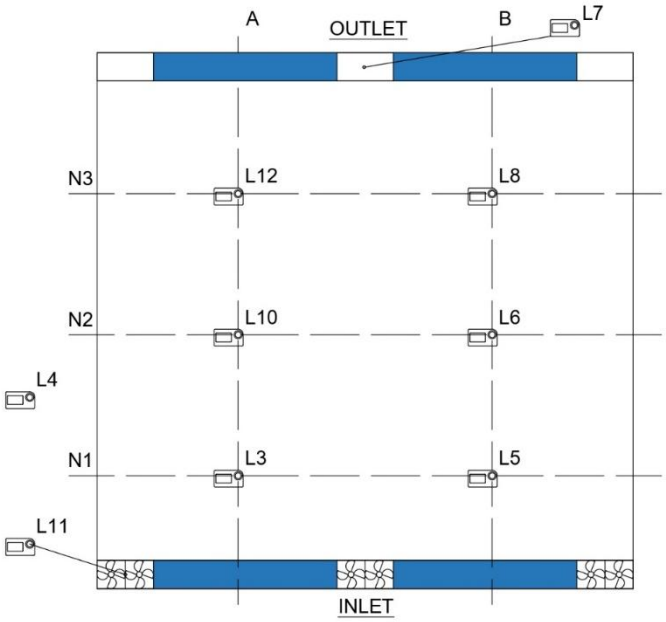


Figure 21: Configuration 6

The outlet openings were matched in size to the inlet area, and, consistent with the fan arrangement, these openings were likewise positioned on either side of the cavity as well as centrally.

Table 10 presents the calculated hourly exchange rate for each individual logger.

Table 10: Results of experiment 10 in ACH (h-1)

Experiment 10	**L11**	**L3**	**L10**	**L12**	**L5**	**L6**	**L8**	**L7**
ACH1	389.0	72.0	83.0	180.0	84.0	148.0	245.0	135.0
ACH2	393.0	75.0	82.0	192.0	81.0	143.0	256.0	129.0
ACH3	374.0	73.0	79.0	165.0	55.0	139.0	211.0	129.0
ACH4	373.0	74.0	77.0	168.0	80.0	139.0	194.0	149.0
ACH5	359.0	82.0	87.0	200.0	67.0	148.0	260.0	151.0
AVG	377.6	75.2	81.6	181.0	73.4	143.4	233.2	138.6

4.2 DISCUSSION OF THE DATA

With the experiments now complete, the results can be summarised as follows: for each logger, the average ACH value was calculated across the repeated cycles of each individual test, thereby providing a single representative ACH value per logger for every experiment conducted. To enable comparison of performance across the individual experiments, the average hourly air exchange rate was calculated using the loggers positioned within the wall cavity, namely loggers L3, L10, L12, L5, L6, and L8. This averaged value is hereafter referred to as the internal AVG. To provide additional clarity, Figure 22 presents a comprehensive overview of the results obtained across all conducted experiments.

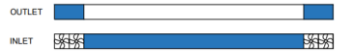
Config.	Image	Experiments	Inlet	Internal						Outlet	Internal
			L11	L3	L10	L12	L5	L6	L8	L7	AVG
Conf 1		Experiment 1 (Chamber off)	275.3	101.0	48.3	98.7	152.0	136.0	176.3	195.3	**118.7**
		Experiment 3	382.0	159.6	70.6	125.2	132.8	144.6	212.4	186.8	**140.9**
Conf 2		Experiment 4	375.0	212.4	80.2	188.6	143.6	135.8	255.6	245.0	**169.4**
Conf 3		Experiment 5	556.6	166.0	95.0	165.6	178.2	139.8	146.6	114.4	**148.5**
		Experiment 9	406.2	120.6	96.4	147.0	154.4	124.6	211.2	89.8	**142.4**
Conf 4		Experiment 6	385.6	138.6	39.6	86.6	111.4	105.0	155.2	182.4	**106.1**
		Experiment 8	394.0	103.0	77.6	114.4	74.0	100.8	167.0	150.0	**106.1**
Conf 5		Experiment 7	418.6	222.4	92.6	93.2	-	124.8	250.6	302.0	**180.9**
Conf 6		Experiment 10	377.6	75.2	81.6	181.0	73.4	143.4	233.2	138.6	**131.3**

Figure 22: Overview of the tests in ACH (h^{-1})

As shown in Figure 22, the configurations that were tested twice, namely Experiments 5 and 9, and Experiments 6 and 8, produced remarkably consistent results in terms of average ACH. Experiments 5 and 9 differed by only 6.1 ACH, despite having been conducted at entirely different points in time, while Experiments 6 and 8 yielded an identical average ACH.

This close agreement between repeated tests indicates a high degree of repeatability in the experimental procedure. For the purposes of the future comparison between configurations, the values obtained from these repeated tests were averaged with one another, resulting in a single representative value for each configuration. It should be noted that Experiments 1 and 3 represent an exception to this pattern, as these two tests were conducted under different climatic chamber statuses and are therefore not directly comparable in the same manner since the stack effect is at play. Such as outlined in Chapter 3, this research aimed to investigate the significance of the stack effect on experimental outcomes. To examine how varying the number of fans and their spatial configuration influences the internal airflow and to determine the most optimal fan arrangement for practical and real world applications.

The initial hypotheses stated that larger openings and an increased number of fans would yield higher airflow rates, while the stack effect was anticipated to exert only a marginal influence on the experimental results. It was further hypothesised that spatially distributing the fans across separate positions along the wall would enhance the internal air changes per hour (ACH), on the assumption that a wider spread of inlet points would promote an even air distribution throughout the cavity. The following sections present the experimental findings that either validate or refute these propositions, with the underlying reasoning for each outcome discussed in turn.

4.2.1 Comparison of the test

As established in Experiment 1, the climatic chamber was deliberately deactivated during testing to isolate and assess the influence that the stack effect might exert on the experimental outcomes, independent of any temperature driven buoyancy effects introduced by the chamber. When compared against Experiment 3, in which the climatic chamber was operational under an otherwise identical configuration, the results reveal a clear and consistent difference in the average ACH recorded, as illustrated in Figure 23.

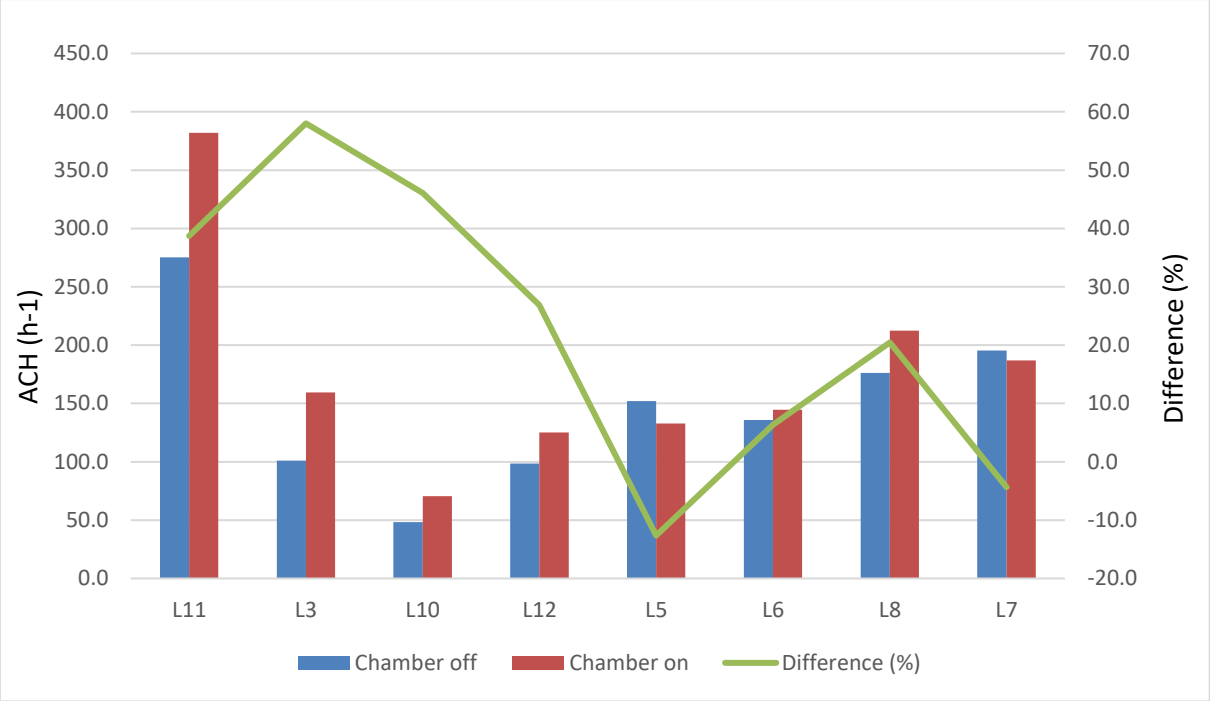


Figure 23: Comparison chamber status

Specifically, activation of the climatic chamber corresponded to a net increase of 18.7% in internal ACH relative to the chamber-inactive condition. Given that the only variable altered between the two experiments was the operational status of the climatic chamber, this increase can be attributed with a reasonable degree of confidence to the temperature differential established across the wall assembly, which in turn drives a buoyancy induced stack effect within the cavity. Warmer air on the chamber side of the wall would be expected to rise and exit through the upper opening, drawing cooler ambient air in through the lower inlet, thereby supplementing the airflow already being generated mechanically by the fans.

This finding is in line with the initial hypothesis that the stack effect would exert only a minor influence on the results. The data suggests that the stack effect makes a modest but measurable contribution to the overall ventilation performance of the system, one that should not be entirely disregarded when interpreting the results of the remaining nine experiments, all of which were conducted with the climatic chamber active. This also implies that the ACH values obtained throughout the majority of this study reflect, to some extent, the combined effect of mechanical ventilation and buoyancy driven airflow, rather than the fan induced airflow in isolation. A distinction worth bearing in mind, although more research would be needed with different configurations to measure the stack effect influence on different setups.

4.2.2 Comparison of the configurations

The experimental results demonstrate that increasing the number of fans has a direct and positive effect on the internal ACH, a finding that is consistent with the initial hypothesis outlined in Chapter 3.

As the total number of active fans increased from two to four, and subsequently from four to six, a corresponding upward trend in ACH was observed across the relevant experiments. This confirms that, within the range tested, fan quantity remains a relevant and effective parameter for improving ventilation performance. Figure 24 is a visual representation of the average internal ACH for each configuration.

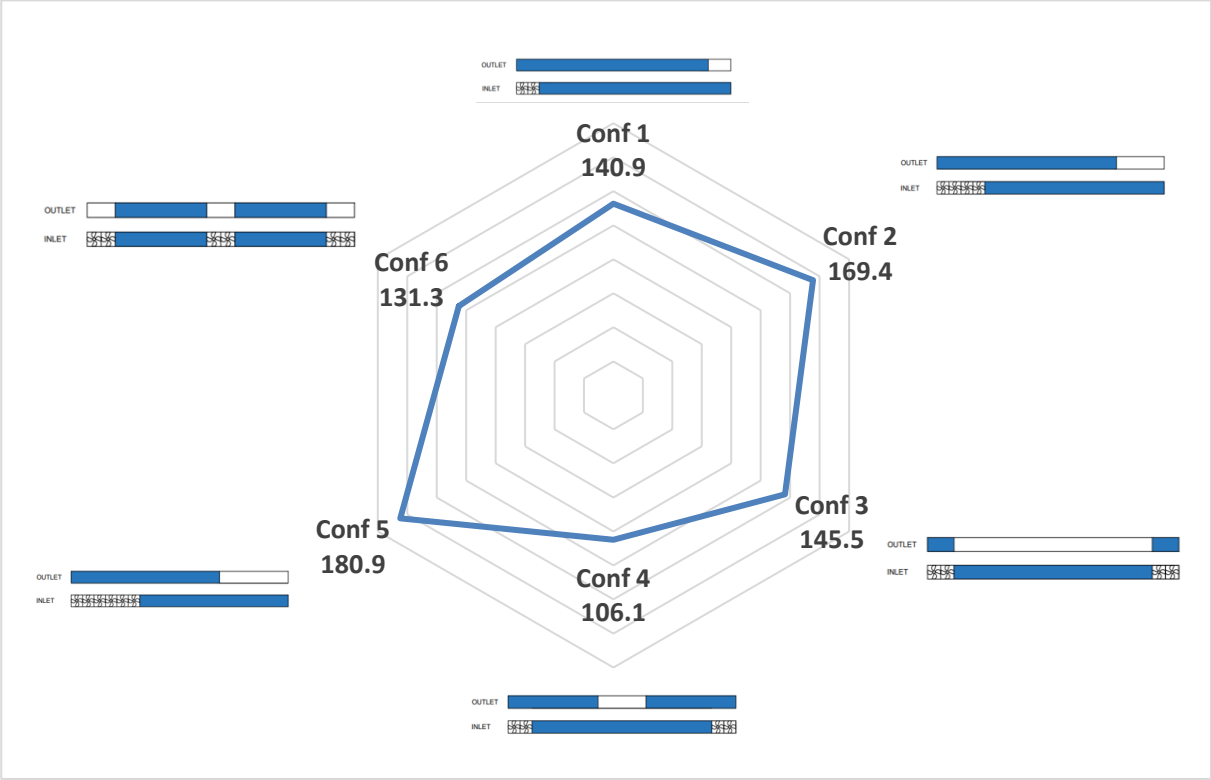


Figure 24: Comparison of the configurations in average ACH (h^{-1})

The spatial configuration of the fans proved to be an equally, if not more, decisive factor in determining overall ventilation performance. Contrary to the initial prediction that distributing fans across separate positions along the wall would yield superior airflow, the experimental data instead reveals that positioning fans adjacently, in a consolidated, side by side arrangement, produced a substantially greater improvement in internal ACH than spacing the same number of fans apart across the wall assembly.

This outcome represents a clear refutation of the second hypothesis and constitutes one of the more significant findings of this research, as it runs counter to the intuitive assumption that a wider distribution of inlet points would necessarily promote more even, and therefore more effective, air distribution throughout the cavity. Figure 25 shows a side-by-side comparison of the configurations where the fans are positioned adjacent and opposing from each other.

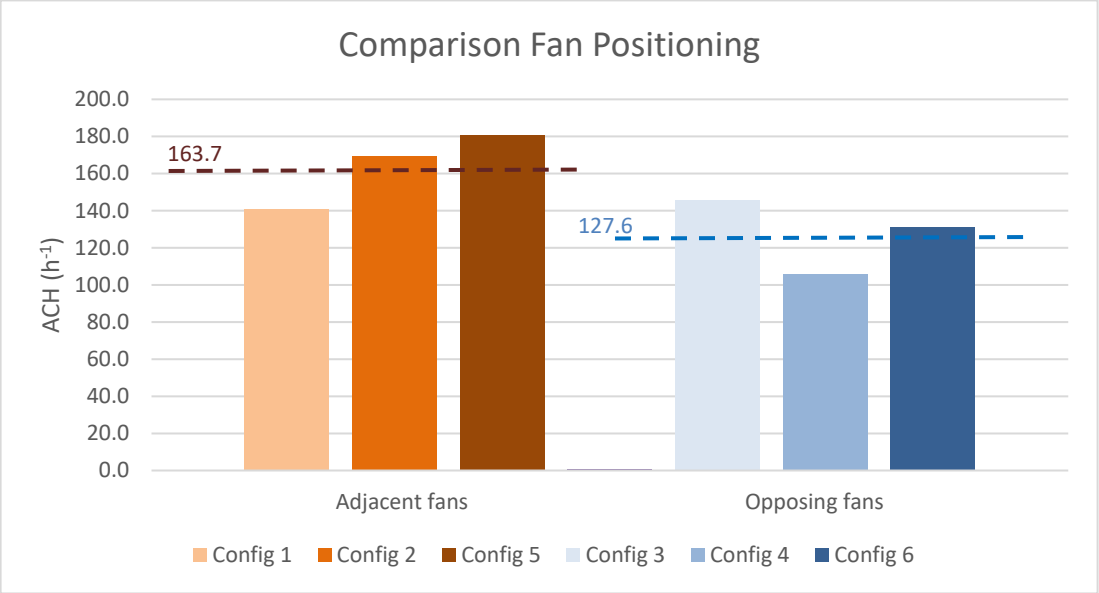


Figure 25: Comparison of positioning of the fans in ACH (h^{-1})

As shown in Figure 25, configurations in which the fans were positioned adjacent to one another yielded an average ACH of 163.7 h^{-1}, compared with an average of 127.6 h^{-1} for configurations in which the fans were positioned on opposite sides of the wall. When Configurations 2 and 4 are compared directly, both employing the same number of fans and the same outlet area, Configuration 2, with its adjacent fan arrangement, achieved an ACH of 169.4 h^{-1}, representing a 59.6% improvement over Configuration 4, with its opposing fan arrangement, which achieved an ACH of 106.1 h^{-1}. A similar pattern was observed when comparing Configuration 5 with Configuration 6, with the adjacent fan arrangement of Configuration 5 outperforming Configuration 6 by 37.8%.

A plausible explanation for this outcome is that the collective airflow generated by adjacent fans creates a compounding effect, whereby the combined pressure differential produced by the grouped configuration drives a more forceful and consistent air movement through the internal cavity of the wall. When fans were instead spatially distributed, the individual airflow streams appeared to operate more independently of one another, reducing the synergistic potential of the combined fan output and ultimately resulting in comparatively lower ACH values.

This behaviour may be attributable to the localised nature of each fan's pressure zone, which, when isolated from neighbouring units, lacks the lateral reinforcement that appears to be present when fans are positioned near one another. In effect, the grouped fans appear to behave less like a set of independent air sources and more like a single, larger effective inlet, generating a stronger and more unified pressure gradient across the cavity than an equivalent number of dispersed fans could achieve individually.

Furthermore, the experiments confirm that a larger opening size contributes positively to the total ACH, as it reduces resistance to airflow and allows a greater volumetric exchange of air within the assembly. When cross comparing configuration 3 and 4. Configuration 3 has a far bigger opening (1500 cm^2) than configuration 4 (400 cm^2). As shown in the results, this larger opening resulted in an increase of 39.40 ACH (h^{-1}), corresponding to a relative improvement of 36.95%.

This finding is consistent with the initial hypothesis and aligns with basic fluid dynamic principles, whereby a reduction in restriction at the outlet permits a given volume of air to pass through the system more readily. However, when the relative magnitude of this effect is compared against that observed for fan adjacency, it becomes evident that opening size, while a relevant and measurable parameter, exerts a secondary influence on ACH relative to fan positioning. In practical terms, this suggests that the gains achieved by widening an opening are comparatively modest when set against the gains achieved by consolidating fan placement, indicating that these two variables should not be treated as equally weighted design considerations.

This distinction carries a meaningful practical implication: when designing ventilation configurations for real world applications, particularly in contexts where space, material, or structural constraints may limit the extent to which openings can be enlarged, the data suggests that greater performance gains are likely to be achieved by prioritising the consolidation and careful positioning of fans, rather than by focusing primarily on maximising opening dimensions. This is a particularly relevant consideration for retrofit or constrained-envelope applications, where increasing opening size may not always be feasible, but where fan layout can typically be adjusted with comparatively greater freedom.

Taken together, these findings highlight fan arrangement as the dominant variable in maximising ventilation efficiency within the tested wall system, ahead of both fan quantity and opening size. The adjacent fan configuration consistently outperformed all other tested arrangements across the experimental conditions examined, establishing it as the most effective and practically viable configuration identified within the scope of this research. These results carry meaningful implications for the design of dynamic thermal insulation systems and ventilated building envelopes more broadly, where spatial constraints and performance requirements must be carefully balanced, and where an informed understanding of the relative importance of fan quantity, fan positioning, and opening size can meaningfully inform more efficient design decisions.

5
CONCLUSION

This thesis investigated the ventilation performance of a dynamic thermal insulation system (DTIS) integrated within a double-leaf wall assembly, focusing on how fan quantity, fan positioning, and opening size influence air changes per hour (ACH) within the wall cavity, and to what extent the stack effect contributes to overall airflow behaviour.

5.1 SUMMARY OF THE METHODOLOGY

The experimental campaign used a double brick leaf wall specimen (1900 x 1900 mm, 403 mm thick), incorporating a 60 mm exterior insulation panel, with a climatic chamber on the rear side providing controlled thermal conditions. Carbon dioxide was used as a tracer gas in accordance with the concentration decay method defined in ISO 12569:2017 [15], monitored with a 6 CO_2 loggers placed inside the wall cavity, two loggers placed at the inlet and outlet with an additional logger placed outside the wall to measure ambient CO2 concentrations. Calibration allowed the most accurate loggers to be identified for use in the main experimental campaign, ensuring reliable and comparable ACH values throughout.

The fan system operated on a 12V DC, with the fans wired in parallel pairs to allow independent activation and free repositioning. In total, six configurations were tested, varying fan quantity of two, four or six. The arrangement of the fans and the opening size of the outlet area could be changed depending on the configuration selection. Each experiment followed a three-phase procedure: the injection, the settlement and the decay. Which were repeated a minimum of five times. The methodology was refined over the course of the campaign, most notably through the introduction of a logarithmic error margin criteria for selecting valid regression data points. This refinement resulted in significant increase in consistency and accuracy.

5.2 RESULTS AND KEY FINDINGS

Comparing Experiment 1 (with the chamber inactive) against Experiment 3 (with the chamber active) with the same configuration, revealed a net increase of 18,7% in internal ACH attributable to the stack effect. This indicates that the buoyancy driven airflow resulting from the temperature differential across the wall made a modest but measurable contribution to overall ventilation performance. Even though the impact was smaller than the contribution of fan configuration or opening size, but still relevant when interpreting the remaining experiments, all conducted with the chamber active.

Increasing fan quantity had a positive effect on internal ACH $^{-1}$ as initially expected. However, fan positioning proved an equally decisive factor. Adjacent fan arrangements consistently outperformed distributed arrangements using the same number of fans. This arrangement achieved a mean ACH of 163.7 h^{-1} compared with 127.6 h^{-1} when the fans were distributed along the wall inlet. This was most evident when comparing Configuration 2 (adjacent, 169.4 h^{-1}) against Configuration 4 (opposing, 106.1 h^{-1}), a 59.6% improvement, with a comparable 37.8% improvement observed between Configuration 5 and Configuration 6.

Opening size also has a positive effect on the internal ACH. Comparing Configuration 3 (1500cm^2) against Configuration 4 (400cm^2) resulted in an increase of 39.40 ACH, a 36.95% improvement. The repeatability and accuracy were confirmed through direct repetition of configurations: Experiments 5 and 9 (Configuration 3), conducted at different times, differed by only 6.1 h^{-1}, while Experiments 6 and 8 (Configuration 4) produced an identical internal average ACH, lending confidence to the reliability of the methodology.

5.3 IMPLICATIONS AND DISCUSSION

These findings indicate that fan positioning is the most influential of the three variables examined, ahead of both fan quantity and opening size. The consistent improvement of adjacent fan arrangements suggests that closely positioned fans generate a stronger, more effective airflow through the cavity than the same number of fans spread apart. This finding does not straightforwardly align with the broader literature on fan and jet interaction, where close spacing is more commonly associated with turbulent losses from jet collision rather than performance gains.

This divergence suggests that the specific cavity geometry, and the relationship between fan placement and opening position, may play an important role, and that this finding should be understood as specific to the tested configuration rather than a universally applicable principle.

Practically, these results suggest that prioritising fan consolidation and positioning is likely to yield greater ventilation performance benefits than simply increasing fan quantity or enlarging openings. Especially in real life applications where spatial or structural constraints limit opening size and positioning.

5.4 RECOMMENDATIONS FOR FUTURE RESEARCH

Future research would benefit from validating the CO2 concentration decay method against an independent measurement technique, such as anemometry, to verify that the ACH values obtained through the tracer gas method accurately reflect the actual airflow velocities within the cavity. Cross-referencing these two approaches would help confirm the reliability of the decay method used in this study and could additionally provide more detailed spatial information on airflow behaviour within the cavity than is achievable through point-based CO2 logging alone.

The present study was further limited to a single fan type operating at a fixed flow rate. Future research could test a range of fan types offering different airflow speeds and pressure characteristics. This would also allow the relative influence of fan positioning to be assessed against fan capacity more directly, providing clearer guidance for selecting and arranging fans in practical applications.

In addition to further laboratory testing, it is recommended that future research extend this work through real life field testing and long-term monitoring of a DTIS walls installed within an existing building. This would enable for cross comparison of in field results with results conducted in the laboratory and how larger walls dimensions fare with the dynamic thermal insulation systems.

REFERENCES

[1] IPCC. (2023). Synthesis report of the IPCC Sixth Assessment Report (AR6) Summary for Policymakers. In IPCC. Intergovernmental Panel on Climate Change. https://www.ipcc.ch/report/ar6/syr/downloads/report/IPCC_AR6_SYR_SPM.pdf

[2] Marando, F., Heris, M. P., Zulian, G., Udías, A., Mentaschi, L., Chrysoulakis, N., Parastatidis, D., & Maes, J. (2022). Urban heat island mitigation by green infrastructure in European Functional Urban Areas. *Sustainable Cities and Society*, *77*(103564), 103564. https://doi.org/10.1016/j.scs.2021.103564

[3] Iungman, T., Cirach, M., Marando, F., Pereira Barboza, E., Khomenko, S., Masselot, P., Quijal-Zamorano, M., Mueller, N., Gasparrini, A., Urquiza, J., Heris, M., Thondoo, M., & Nieuwenhuijsen, M. (2023). Cooling Cities through Urban Green infrastructure: a Health Impact Assessment of European Cities. The Lancet, 401(10376), 577–589. https://doi.org/10.1016/s0140-6736(22)02585-5

[4] Exposure of social infrastructure to flooding and UHI. (2026, March 6). Europa.eu. https://climate-adapt.eea.europa.eu/en/observatory/publications-data/analysis-data/exposure-of-social-infrastructure

[5] e-Prime - Advances in Electrical Engineering, Electronics and Energy | Journal | ScienceDirect.com by Elsevier. (n.d.). Www.sciencedirect.com. https://www.sciencedirect.com/journal/e-prime-advances-in-electrical-engineering-electronics-and-energy

[6] Not just another brick in the wall: The solutions exist - Scaling them will build on progress and cut emissions fast. Global Status Report for Buildings and Construction 2024/2025. (2025). https://doi.org/10.59117/20.500.11822/47214

[7] The Future of Cooling Opportunities for energy- efficient air conditioning Together Secure Sustainable. (n.d.). https://iea.blob.core.windows.net/assets/0bb45525-277f-4c9c-8d0c-9c0cb5e7d525/The_Future_of_Cooling.pdf

[8] World. (2024, October 16). *World Energy Outlook 2024 – Analysis - IEA*. IEA. https://www.iea.org/reports/world-energy-outlook-2024#overview

[9] Karanafti, A., Theodosiou, T., & Tsikaloudaki, K. (2022). Assessment of buildings' dynamic thermal insulation technologies: A review. Applied Energy, 326, 119985.. https://doi.org/10.1016/j.apenergy.2022.119985

[10] Almeida, R. M. S. F., Teles-Ribeiro, M., & Barreira, E. (2023). Characterization of a wall system with dynamic thermal insulation: Experimental campaign and numerical simulation. Energies, 16(17), 6402.. https://doi.org/10.3390/en16176402

[11] Attia, S., Bilir, S., Safy, T., Struck, C., Loonen, R., & Goia, F. (2018). Current trends and future challenges in the performance assessment of adaptive facade systems. Energy and Buildings, 179, 165-182.. https://doi.org/10.1016/j.enbuild.2018.09.017

[12] Aelenei, D., Aelenei, L., & Vieira, C. (2016). Adaptive facade: Concept, applications, research questions. Energy Procedia, 91, 269-275.. https://doi.org/10.1016/j.egypro.2016.06.218

[13] Loonen, R. C. G. M., Trcka, M., Costola, D., & Hensen, J. L. M. (2013). Climate adaptive building shells: State-of-the-art and future challenges. Renewable and Sustainable Energy Reviews, 25, 483-493.. https://doi.org/10.1016/j.rser.2013.05.010

[14] Fawaier, M., & Bokor, B. (2022). Dynamic insulation systems of building envelopes: A review. Energy and Buildings, 270, 112268.. https://doi.org/10.1016/j.enbuild.2022.112268

[15] International Organization for Standardization. (2017). ISO 12569:2017: Thermal performance of buildings and materials - Determination of specific airflow rate in buildings - Tracer gas dilution method. ISO.. https://www.iso.org/standard/69817.html

[16] Sherman, M. H. (1990). Tracer-gas techniques for measuring ventilation in a single zone. Building and Environment, 25(4), 365-374.. https://doi.org/10.1016/0360-1323(90)90010-O

[17] Cui, S., Cohen, M., Stabat, P., & Marchio, D. (2015). CO2 tracer gas concentration decay method for measuring air change rate. Building and Environment, 84, 162-169.. https://doi.org/10.1016/j.buildenv.2014.11.007

[18] Tablada, A., De Troyer, F., Blocken, B., Carmeliet, J., & Verschure, H. (2009). On natural ventilation and thermal comfort in compact urban environments - the Old Havana case. Building and Environment, 44(9), 1943-1958.. https://doi.org/10.1016/j.buildenv.2009.01.008

[19] Hazim Awbi, Ventilation of Buildings. (2023). https://azaranstore.com/wp-content/uploads/2022/09/199-Ventilation-of-Buildings-2003.pdf